

Company : URS/NETL

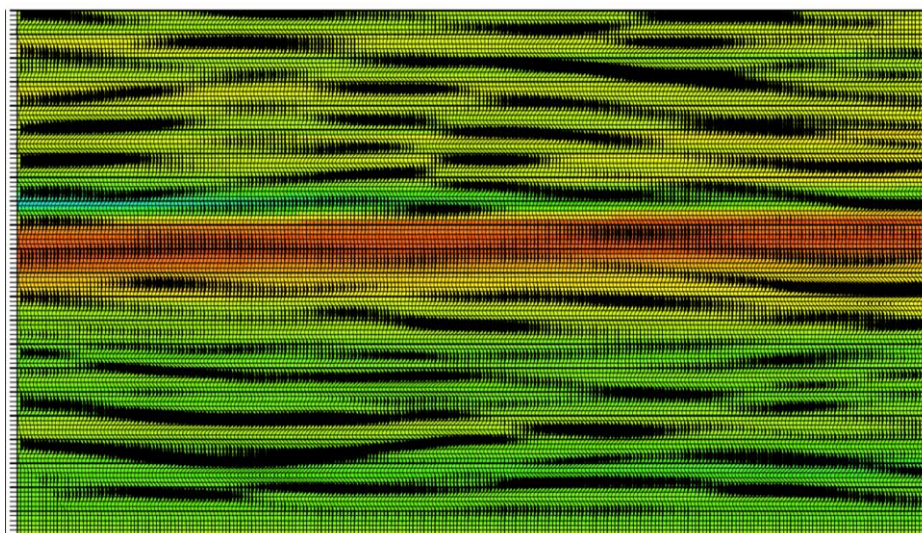
Field : COP 324

County : Clearfield County, Pennsylvania

Acquisition Date : July 2013

Job Number : 784

Revision Number: Revision 2



SEPTEMBER, 2013
REVISION 2

Table of Contents

EXECUTIVE SUMMARY	2
Introduction	2
Data Acquisition	3
Data Processing	4
Results	5
DATA ACQUISITION	9
Acquisition Summary	9
DATA PROCESSING	15
Data Preparation	15
Tomographic Processing	17
First-Arrival Identification	17
First-Arrival Picking	17
Traveltime Tomography Summary Description	20
Final Inversion	32
Pixelized Difference Tomography	36
Reflection Imaging	40
Wavefield Separation	41
Deconvolution and Amplitude Normalization	46
VSP-CDP Mapping/Time-Depth Conversion	49
Post-Map Migration	49
Angle Selection and Stacking	49
Data Enhancement	51
APPENDIX A – TOMOGRAPHIC INVERSION	
APPENDIX B – REFLECTION IMAGING	
APPENDIX C – ANISOTROPY PROCESSING	
APPENDIX D – SURVEY LOGS	
CROSSWELL METHODS & GLOSSARY	

EXECUTIVE SUMMARY

Introduction

Schlumberger's DeepLook group successfully completed an integrated crosswell seismic project for URS/NETL in Clearfield County, Pennsylvania. The project involves acquiring a crosswell seismic profile to image reservoir conditions pre- and post-hydraulic fracture and to provide a high resolution image of the reservoir. The project will occur on the COP 324 pad in Clearfield County, Pennsylvania and consist of 1 non-perforated monitor well with one non-perforated transmitter well nearby.

The acquisition plan deployed a 20-level VSI array in well COP 324#6 and the Z-Trac source in well COP 324#4. Data acquisition was conducted between the source and the receiver wells before the hydraulic fracture and again after the procedure, resulting in 2 profiles total. Once the baseline crosswell profile is acquired the source was rigged down and a 12-level VSI array was deployed for 4 days to record the Hydraulic Fracture Monitoring (HFM). When the HFM job was completed, the Z-Trac source was rigged up and deployed again in well COP 324#4 and the repeat crosswell survey was recorded.

The objectives of the project are to:

- Identify faults and/or fractures
- Identify the top and thickness of each of the following formations: Onondaga Limestone, Marcellus Shale and Tully Limestone

This report describes the standard tomography results, the reflection imaging of the crosswell profile, and the difference tomography results calculated from the changes between the baseline and repeat surveys.

COP 324 PROJECT

Data Acquisition

On July 11, 2013, Schlumberger's DeepLook group acquired a baseline data set for profile COP 324#6 – COP 324#4 for URS/NETL, in Clearfield County, Pennsylvania. On July 20, 2013, a repeat survey was executed for profile COP 324#6 – COP 324#4 after completion of a Hydraulic Fracture Monitoring (HFM) job. During the acquisition of this profile, the COP 324#6 well held the receiver array, while the source occupied well COP 324#4. Within the zone of interest, the well-to-well distance for profile COP 324#6 – COP 324#4 was approximately 2490 ft. The signal-to-noise ratio (SNR) in the data collected for COP 324#6 – COP 324#4 was moderate, yielding apparent direct arrivals and reflections.

The well locations are displayed in Figure I-1 below.

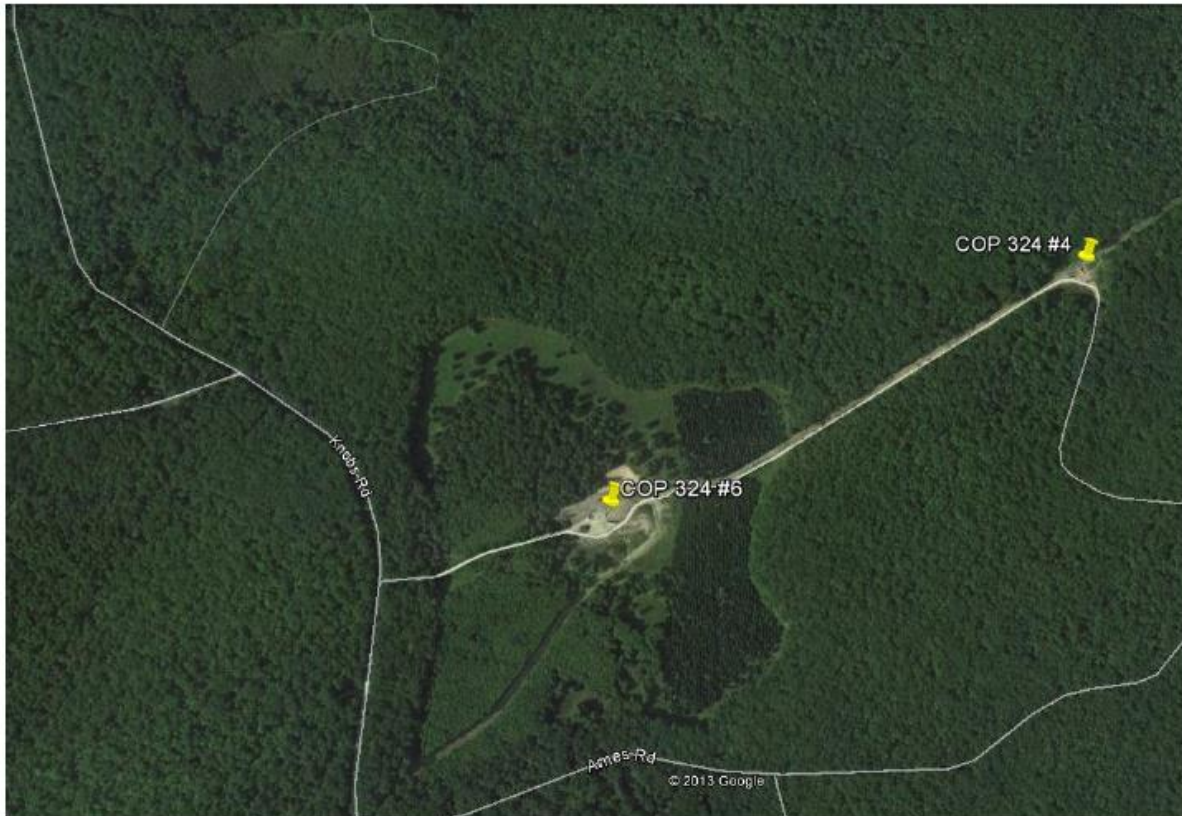


Figure I-1. Map of COP 324 Area.

At the onset of data acquisition, DeepLook lowered the source (well COP 324#4) and receiver array (well COP 324#6) to the deepest levels in their respective wells. The source was

continually swept and raised so that 16 sweeps were recorded at each 50ft interval. These 16 sweeps per source-level were later stacked to a single trace to increase the SNR. When the source reached its shallowest prescribed level, it was lowered back to total depth (TD) while the receiver was raised 50ft and the process was repeated. This method was continued until all required source and receiver positions were occupied by the appropriate tool. The result was a data set with a 50ft source and a 50ft receiver trace increment with a 16-fold stack.

Data Processing

After the data were acquired, it was delivered to DeepLook's Houston offices for crosswell seismic data processing. The crosswell data processing resulted in the crosswell images described in this report, including:

- Compressional Velocity Images from Traveltime Tomography
- Compressional Reflection Stacked Sections
- Compressional Difference Tomography
- Shear Velocity Images from Traveltime Tomography
- Shear Difference Tomography

The data processing sequence that produced the crosswell images included the following steps:

- Data Preparation (Stacking and Correlation)
- Data Component Rotation
- Spectral Analysis
- Tomographic Processing
 - P-Wave First Break Picking
 - P-Wave Traveltime Inversion
 - Shear Wave First Break Picking
 - Shear Wave Traveltime Inversion
- Wavefield separation
 - Direct Arrival Removal
 - Down-going Reflection Removal
- Deconvolution and Amplitude Normalization
- VSP-CDP Transform
- Pre-stack Migration
- Angle Transform
- Angle Selection and Stacking
- Image Post-Processing
- Differencing of the Baseline and Repeat First-Arrival Time Picks
- Difference Tomography

Results

In summary, the crosswell seismic method provided high frequency seismic data with frequencies up to 400 Hz. Two fundamental measurements from the crosswell data volume, velocity and reflectivity were used to provide a robust suite of images to better characterize the reservoir with resolution of 10 to 15 feet. Figures I-2 through I-7 illustrate the resulting velocity and composite images for both the baseline and repeat data sets, while Figures I-8 and I-9 show the difference tomography results for the repeat profiles.

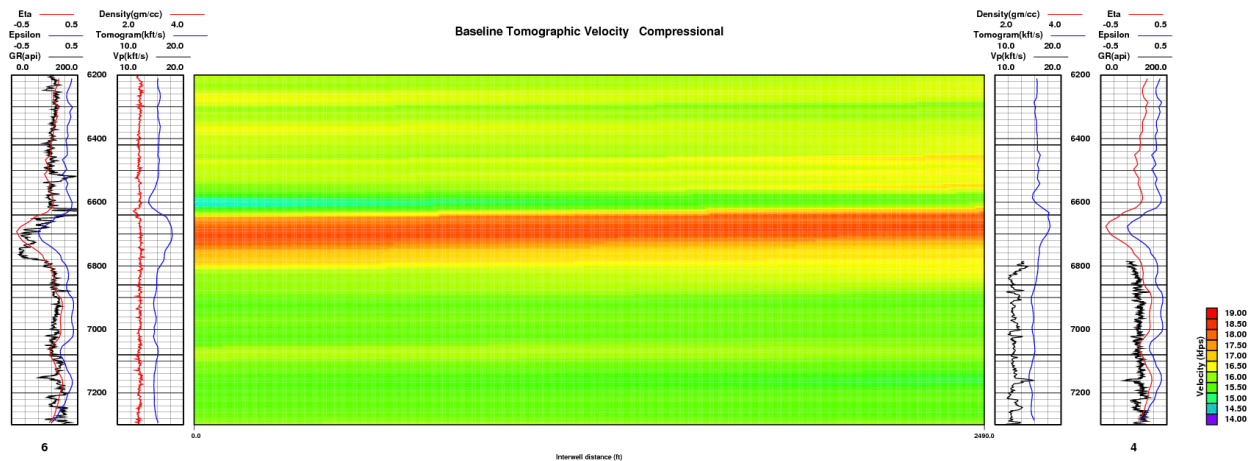


Figure I-2. Baseline Direct-Arrival Tomographic Results for Compressional Wavefield

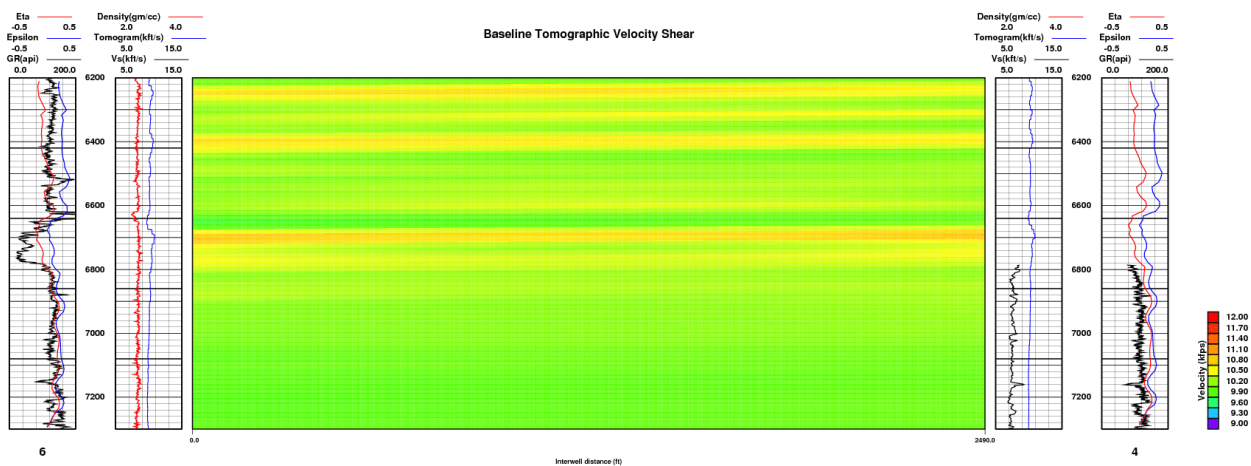


Figure I-3. Baseline Direct-Arrival Tomographic Results for Shear Wavefield

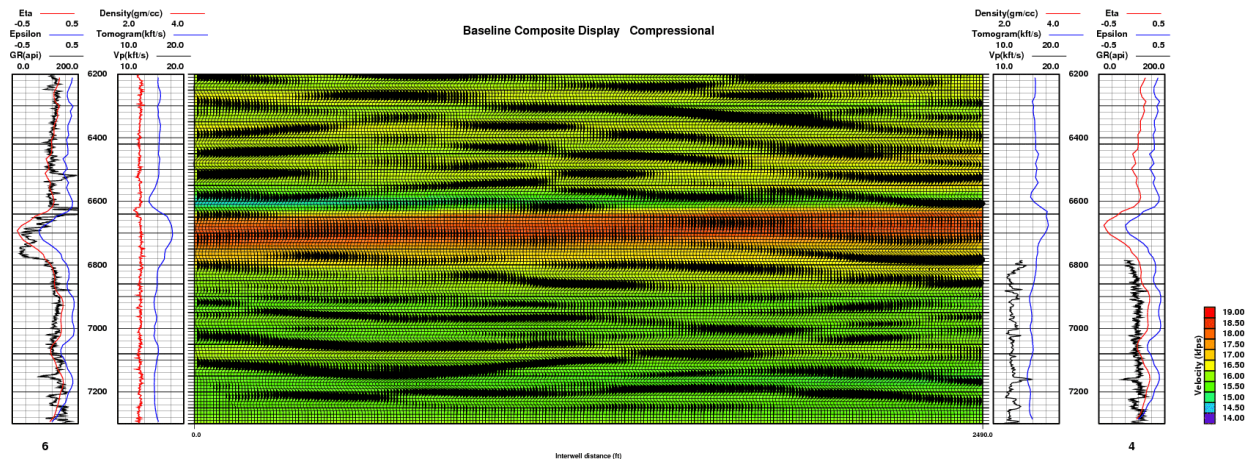


Figure I-4. Baseline Direct-Arrival Composite Results for Compressional Wavefield

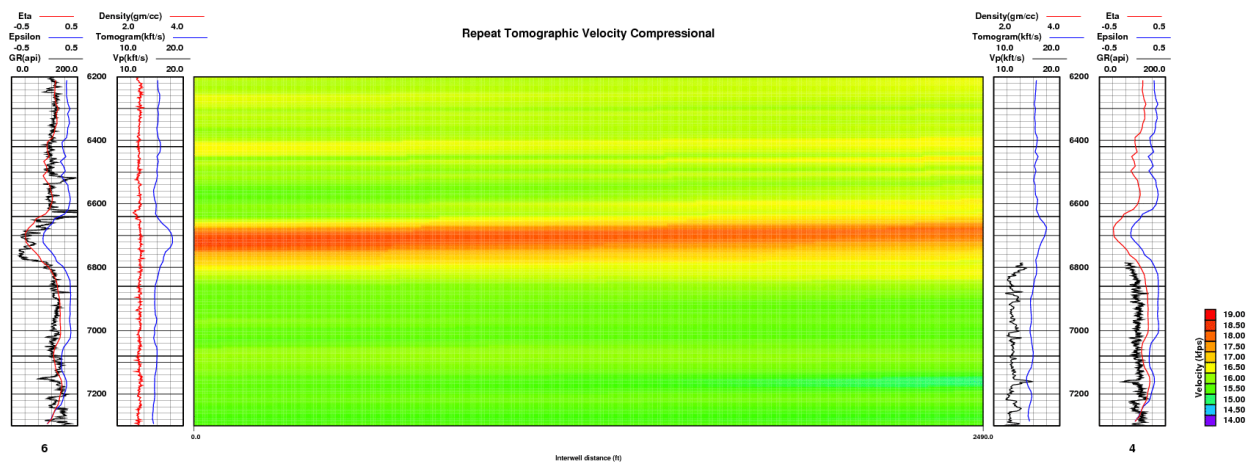


Figure I-5. Repeat Direct-Arrival Tomographic Results for Compressional Wavefield

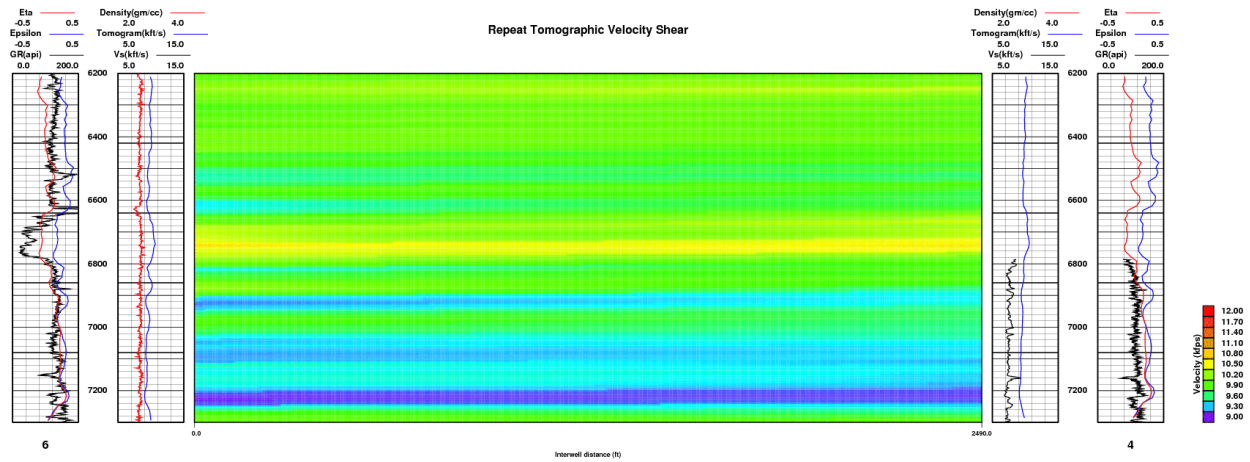


Figure I-6. Repeat Direct-Arrival Tomographic Results for Shear Wavefield

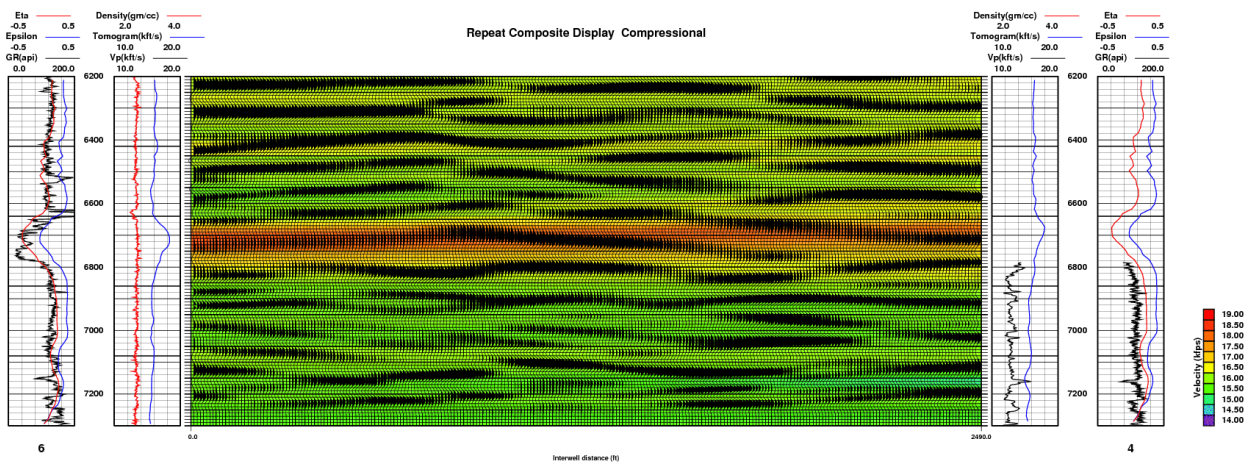


Figure I-7. Repeat Direct-Arrival Composite Results for Compressional Wavefield

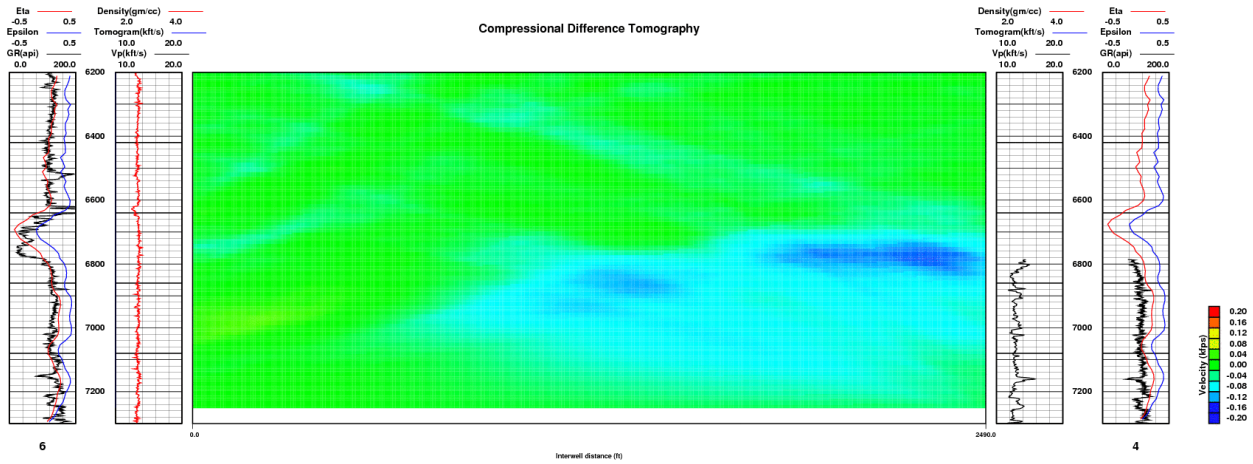


Figure I-8. Pixelized Difference Composite Results for Compressional Wavefiled

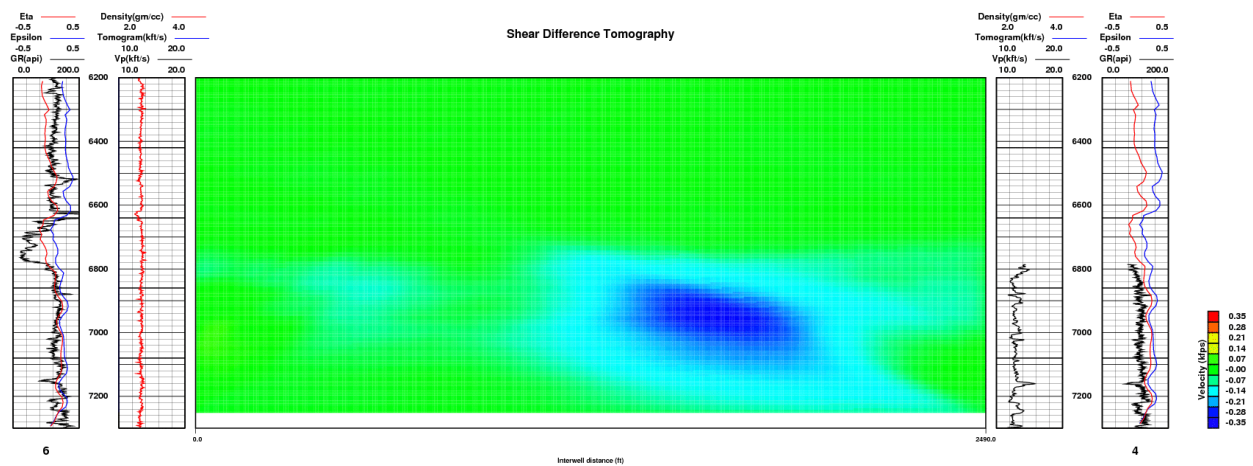


Figure I-9. Pixelized Difference Composite Results for Shear Wavefiled

DATA ACQUISITION

Acquisition Summary

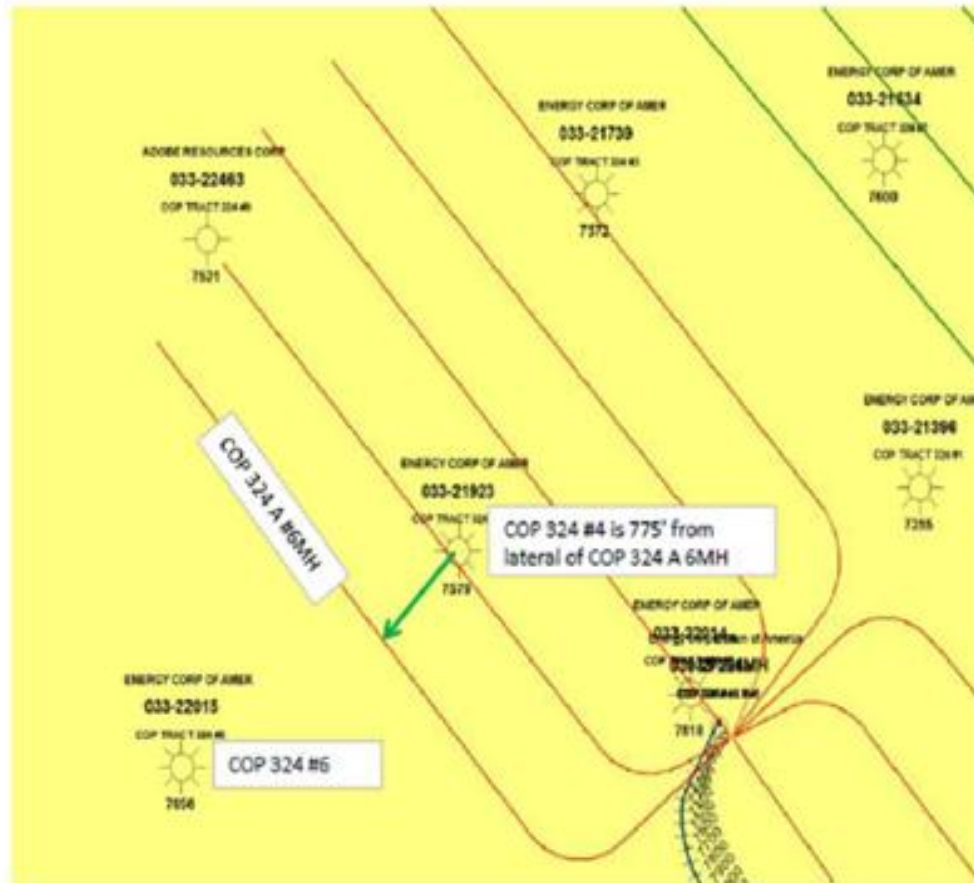


Figure II-1. Map of the COP 324 Well Locations.

Before operations, all Schlumberger crewmembers and 3rd party personnel were involved in a rigorous pre-job safety meeting. After the first overall job safety meeting, a smaller safety meeting was held at each crew change, which involved the Schlumberger crew and any other party on location.

A general summary of the operations method of shooting a crosswell seismic profile follows.

Using the selected parameters, crosswell seismic data were acquired for this survey (See Table II-1). First, the source and receiver array were lowered to TD in their respective wells. The 20-level receiver array remained stationary in the receiver well and the source was slowly raised in the source well. As the source was raised, it was swept with the frequency determined to be most suitable for the profile and noise conditions (30-400Hz). The combination of sweeping the source while raising it resulted in multiple sweeps being recorded over each 50ft interval in the

source well. The source continued to be swept and raised until the top depth described in the shooting plan was achieved. At this point, the source was stopped and sweeping of the source ended. The data set collected by making a traverse of the source in the well while being recorded by the receiver array is termed a fan.

After a fan was completed, the source was lowered to the deepest prescribed depth in the survey plan and the receivers were raised 50ft. The process was then repeated until the source and receivers occupied the shallowest prescribed positions as defined by the survey plan. Data acquisition was complete after all the required fans had been acquired.

The same procedure was repeated after the HFM operation for the repeat line with the same parameters.

The following table lists the actual parameters used in this project.

Parameter	COP 324#6-COP 324#4
Sample Rate (ms)	1.00
Sweep Length (ms)	10400
Sweep Frequency (Hz)	30-400
Record Length (ms)	11200
Correlated Record Length (ms)	800
Interwell Distance (ft)	2490
Sweeps per source interval	16
Source Interval (MD)(ft)	50
Receiver Interval (MD)(ft)	50
Receiver Start Depth (MD)(ft)	6350
Receiver End Depth (MD)(ft)	7250
Source Start Depth (MD)(ft)	4925
Source End Depth (MD)(ft)	7225

Table II-1. Acquisition Parameters.

Displays of a raw receiver and source gather for COP 324#6- COP 324#4 profile (Baseline vs. Repeat) are shown below in Figures II-3 and 5 as well as the acquisition shooting charts for both the baseline and repeat profiles in Figures II-2 and 4.

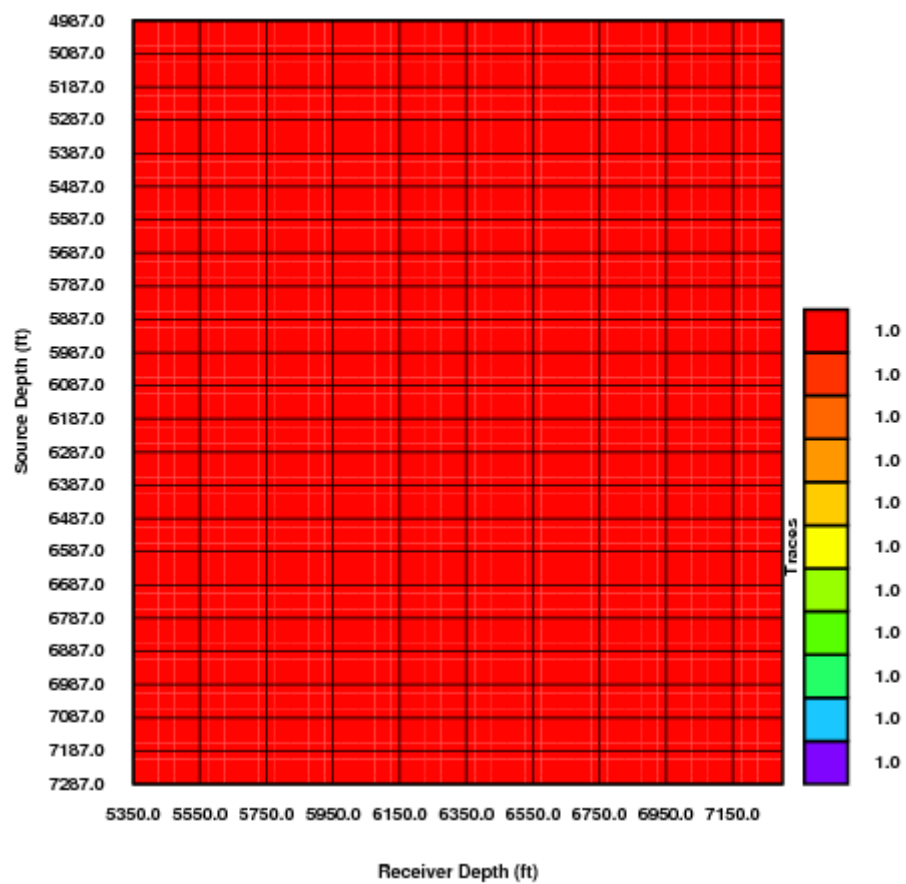
COP_324 6 - COP_324 4 Baseline Shooting Chart

Figure II-2. Baseline Acquisition Shooting Chart.

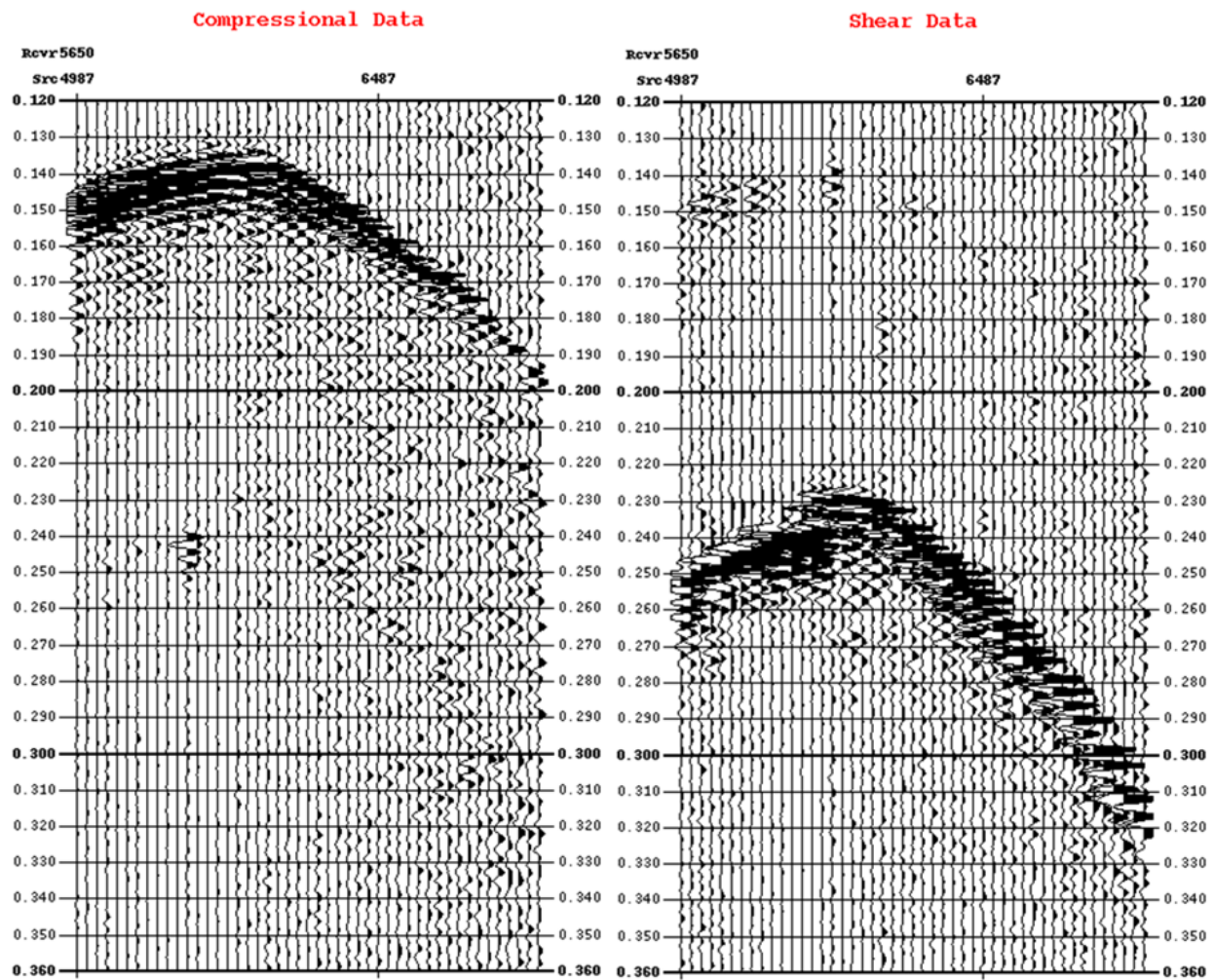


Figure II-3. Baseline Raw Receiver Gather.

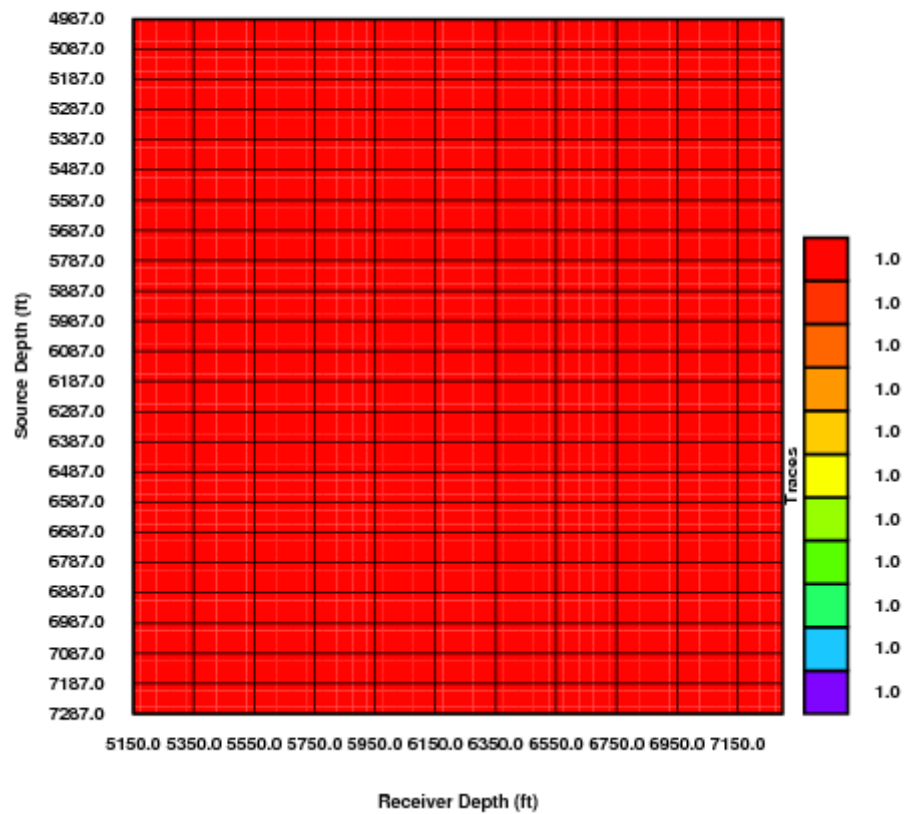
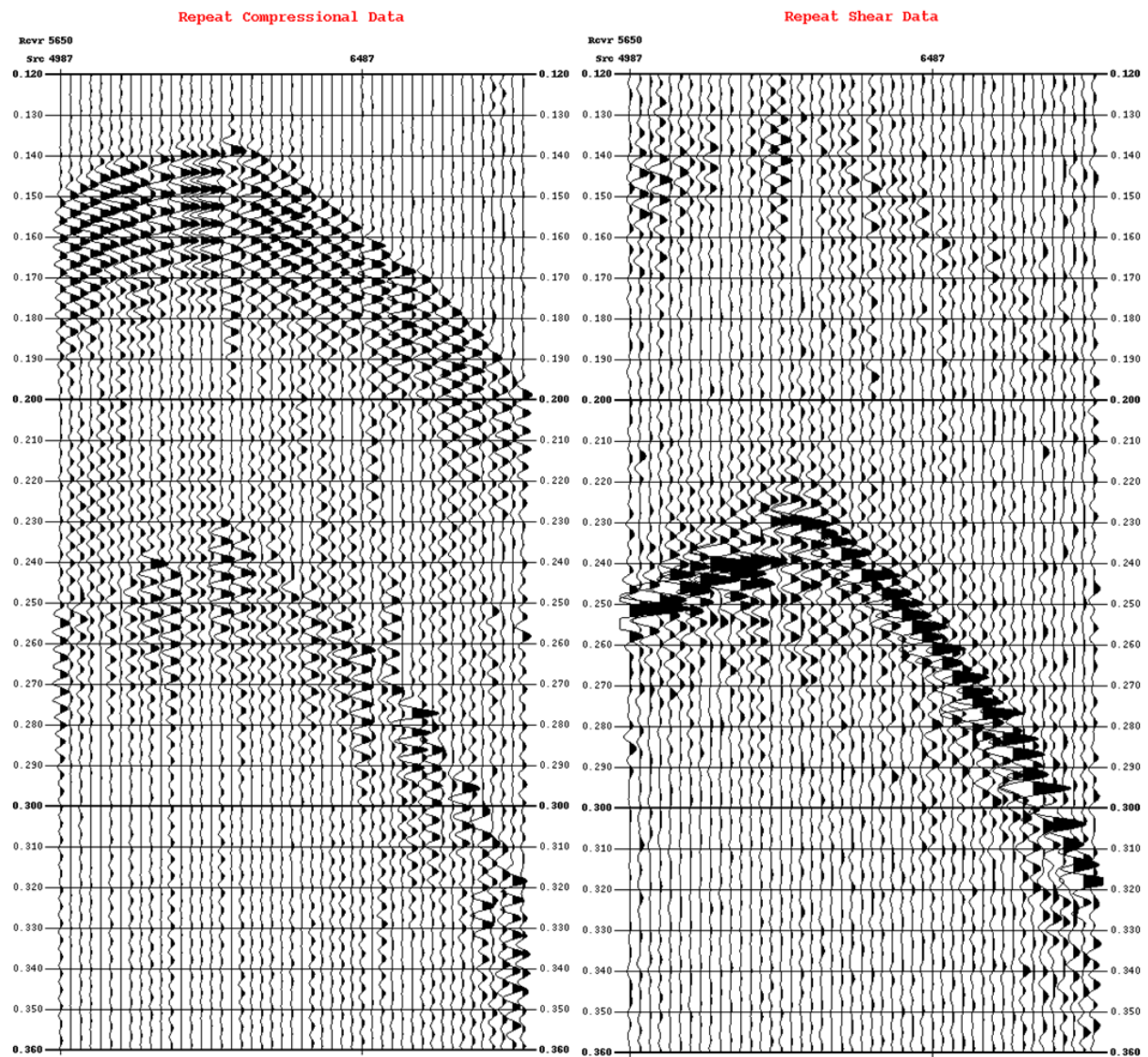
COP_324 6 - COP_324 4 Repeat Shooting Chart

Figure II-4. Repeat Acquisition Shooting Chart.



DATA PROCESSING

Data Preparation

The data processing began with the field data being converted to SEG-Y format and crosswell header locations fully populated. Each trace was noise edited with diversity stacking and cross-correlated with the pilot sweep from 30 to 400 Hz. The result was a stacked and correlated dataset, with a 50 ft depth increment in both the source and receiver well for each of the project profiles. The data were depth adjusted to correspond to URS/NETL's tie-in logs by comparing DeepLook's tie-in logs (a gamma ray log) with the URS/NETL-supplied tie-in logs. The data were then placed on a datum of 2173.0 ft above mean sea level for data processing.

The hardware used for the COP 324 project was DeepLook's Z-Track source coupled with a 20-level array of down-hole geophone receivers. Figures III-1 and III-2 present a typical stacked and correlated receiver gather for both the baseline and repeat profiles, respectively.

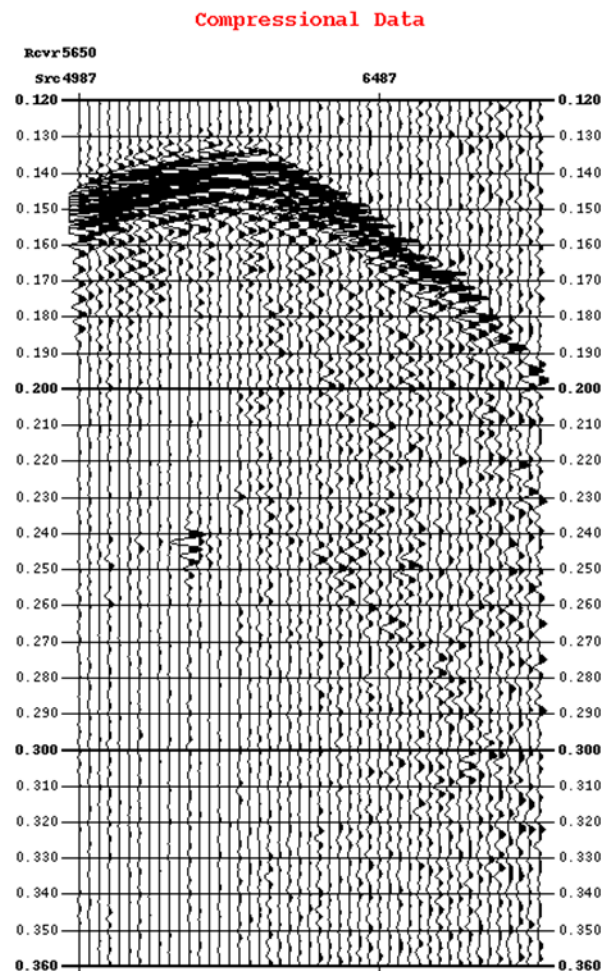
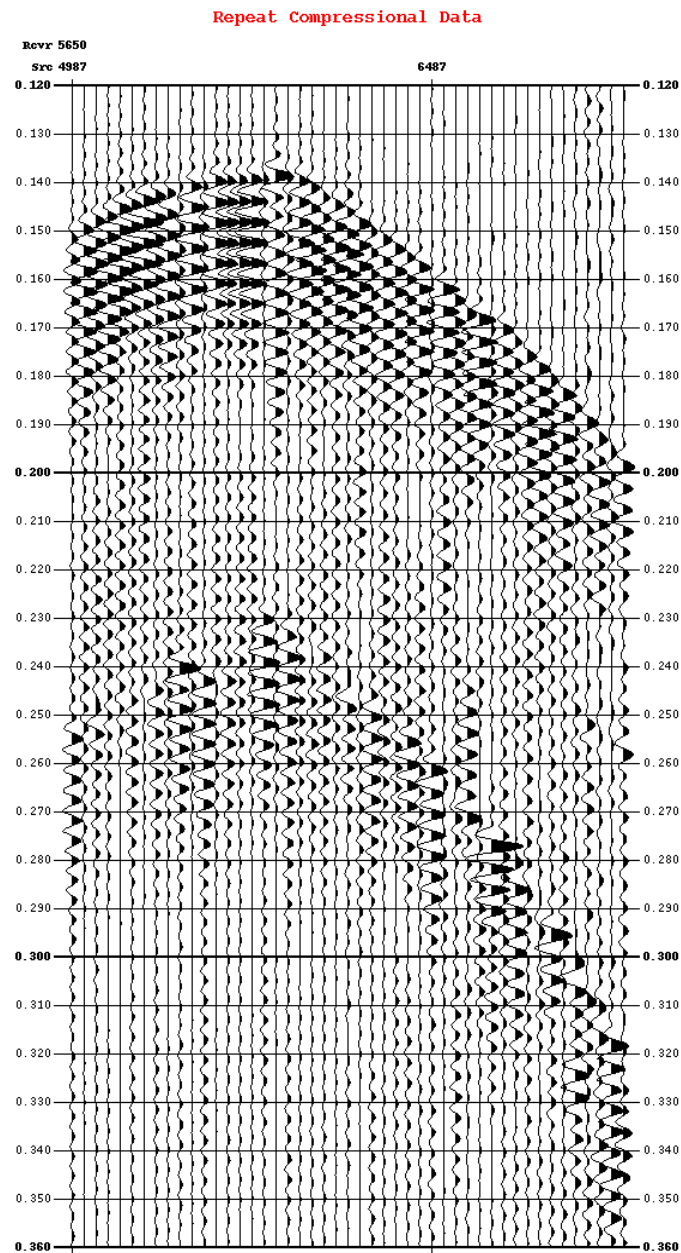


Figure III-1. Stacked and Correlated Baseline Raw Receiver Gather.



Tomographic Processing

Standard tomographic processing was performed for COP 324#6 –COP 324#4 profile. This processing allows for comparison of standard result velocity inspections and is later used as the velocity model for reflection imaging as well as for difference tomography.

Appendix A gives an in-depth description of traveltime tomography and Appendix C gives an in-depth description of the anisotropy estimation made within the traveltime tomography calculations.

First-Arrival Identification

A zero-phase bandpass filter was applied to stabilize the direct-arrival waveform prior to first-break picking. A zero-phase bandpass Ormsby filter with response 30-40-300-400 was used for first-arrival picking only.

First-Arrival Picking

P-wave first-arrivals were identified and picked in four domains:

- Common Receiver
- Common Source
- Common Offset (receiver depth – source depth)
- Common Mid-depth (receiver depth + source depth)/2.

The first-arrival was picked to provide traveltimes for the tomographic inversion. Figure III-3 and Figure III-4 are examples of a common -receiver gather from the baseline and repeat profiles with the traveltime *P*-wave first-arrival picks in green, the final anisotropic tomographic velocity raytraced traveltimes in red for both Baseline and repeat profile. Notice the difference between the two sets of traveltimes are nearly identical, indicating the inversion solution matches the velocity picks. Figures III-5 and III-6 illustrate the same traveltime results for the shear data.

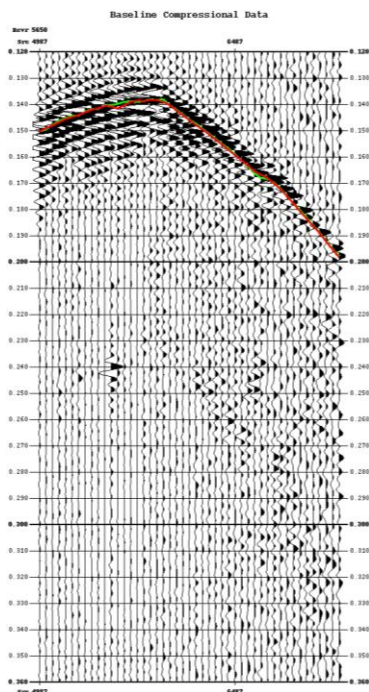


Figure-III 3. Baseline Common Receiver Gather with Both P-Wave and Ray-Traced Direct-Arrival Times.

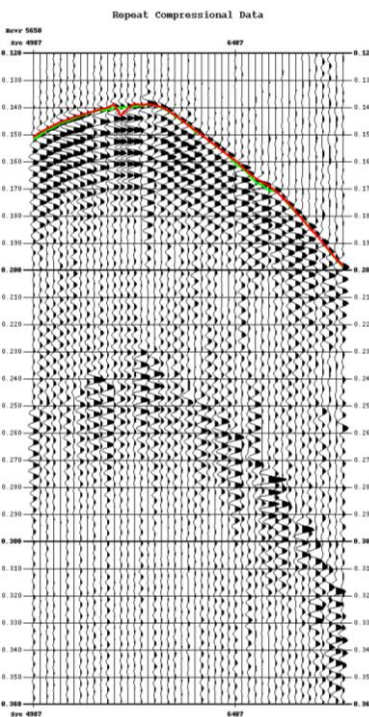


Figure-III 4. Repeat Common Receiver Gather with Both P-Wave and Ray-Traced Direct-Arrival Times.

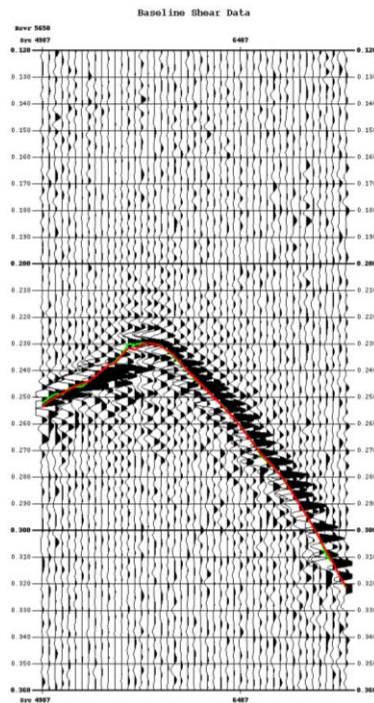


Figure-III 5. Baseline Common Receiver Gather with Both S-Wave and Ray-Traced Direct-Arrival Times.

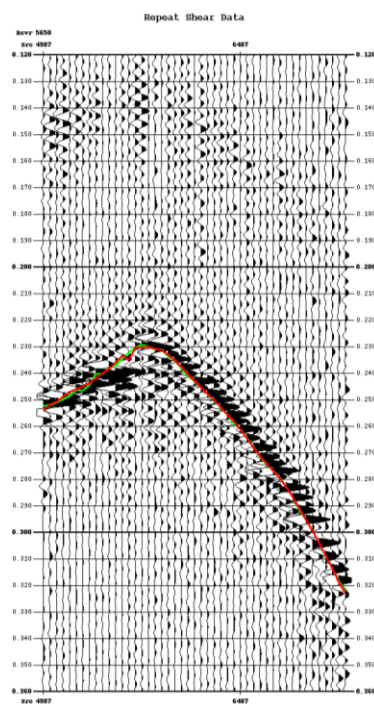


Figure-III 6. Repeat Common Receiver Gather with Both S-Wave and Ray-Traced Direct-Arrival Times.

Traveltime Tomography Summary Description

The 3-D anisotropic traveltime tomography algorithm operates in a rectangular coordinate system with the vertical axis being true vertical depth (TVD). Velocity image values are positioned in the rectangular depth coordinate system. Figures III-7 & 8 show the input direct-arrival traveltimes for the baseline velocity images. Purple indicates no picks were made due to low SNR or wavefield complexity. Figures III-9 and III-10 illustrate the picks made for the repeat profiles.

1. *Baseline P-wave First-Arrival Times*

COP_324 6 - COP_324 4 Baseline Compressional Picks

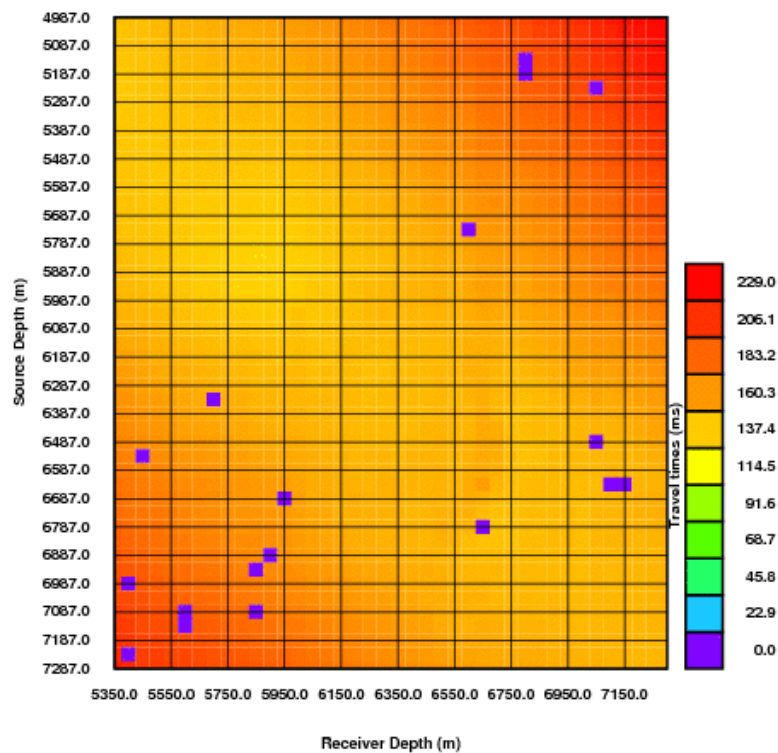


Figure III-7. Baseline: Compressional First-Arrival Times.

COP_324 6 - COP_324 4 Baseline Shear Picks

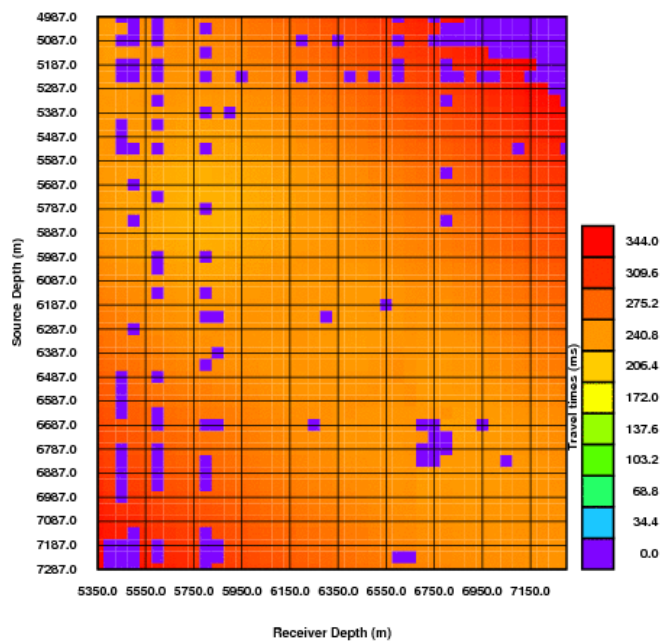


Figure III-8. Baseline: Shear First-Arrival Times.

2. Repeat P-Wave First-Arrival Times.

COP_324 6 - COP_324 4 Repeat Compressional Picks

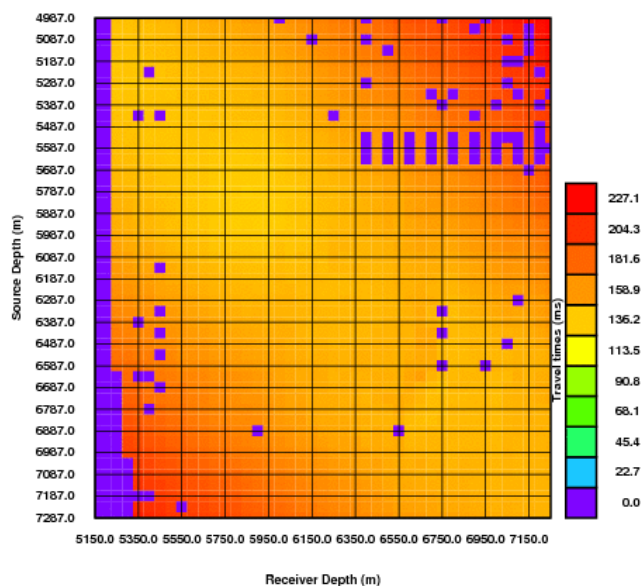


Figure III-9. Repeat: Compressional First-Arrival Times.

COP_324 6 - COP_324 4 Repeat Shear Picks

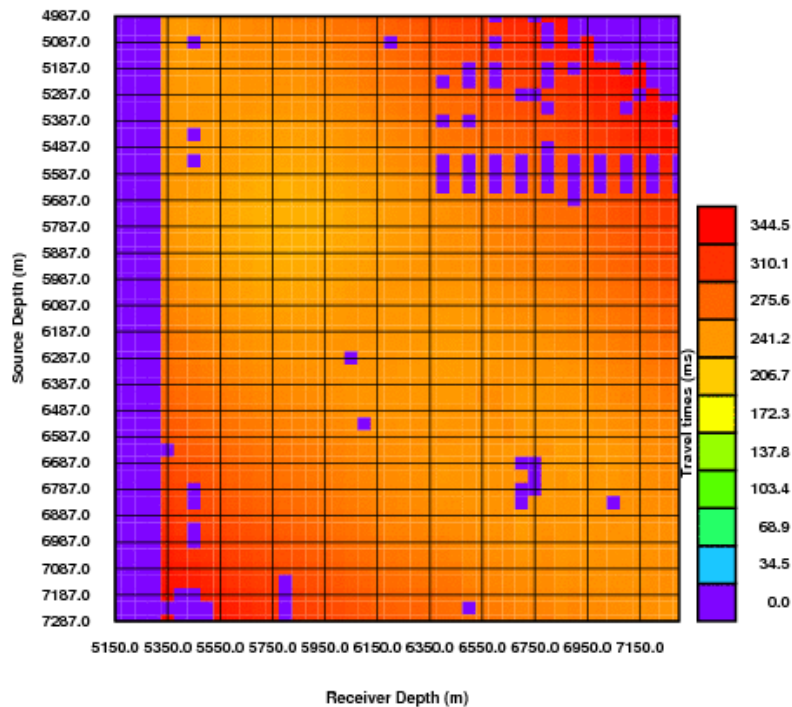


Figure III-10. Repeat: Shear First-Arrival Times.

3. **Receiver and Source Locations.** These are based on the deviation survey information available. The accuracy of the velocity values depends upon the precision of the deviation survey information.
4. **Structural Model.** The starting structure model used for the tomography is derived from formation tops, horizon picks or other geologic information. A surface is fit to these horizon picks at each well. Depending on the complexity of the geology, a first order, second order, or third order polynomial surface is used (Figure III-11).

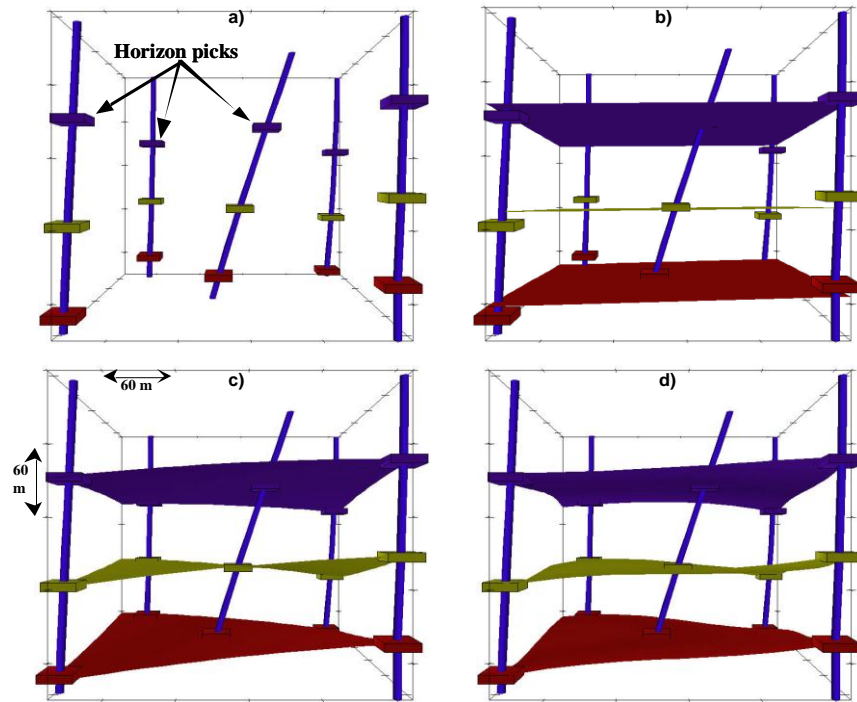


Figure III-11. A general example of wells with horizon picks (a). First (b), second (c) and third (d) order polynomial surfaces fit to the horizon picks of each well.

5. **Isotropic Parameter Selection.** Parameter selection, which allows the calculated tomographic velocity model to be either isotropic or anisotropic, is input to the inversion routine. Appendix A and Appendix C discuss traveltime tomography and anisotropic processing respectively.

The starting model is raytraced and traveltimes are calculated (see example in Figure III-12). The calculated traveltimes are compared with the measured traveltimes and the starting model is updated through a series of non-linear continuation steps to minimize the traveltime residuals (difference between the first-arrival picks and calculated traveltimes). Anisotropic parameter settings were considered and used for tomographic velocity calculations and reflection imaging.

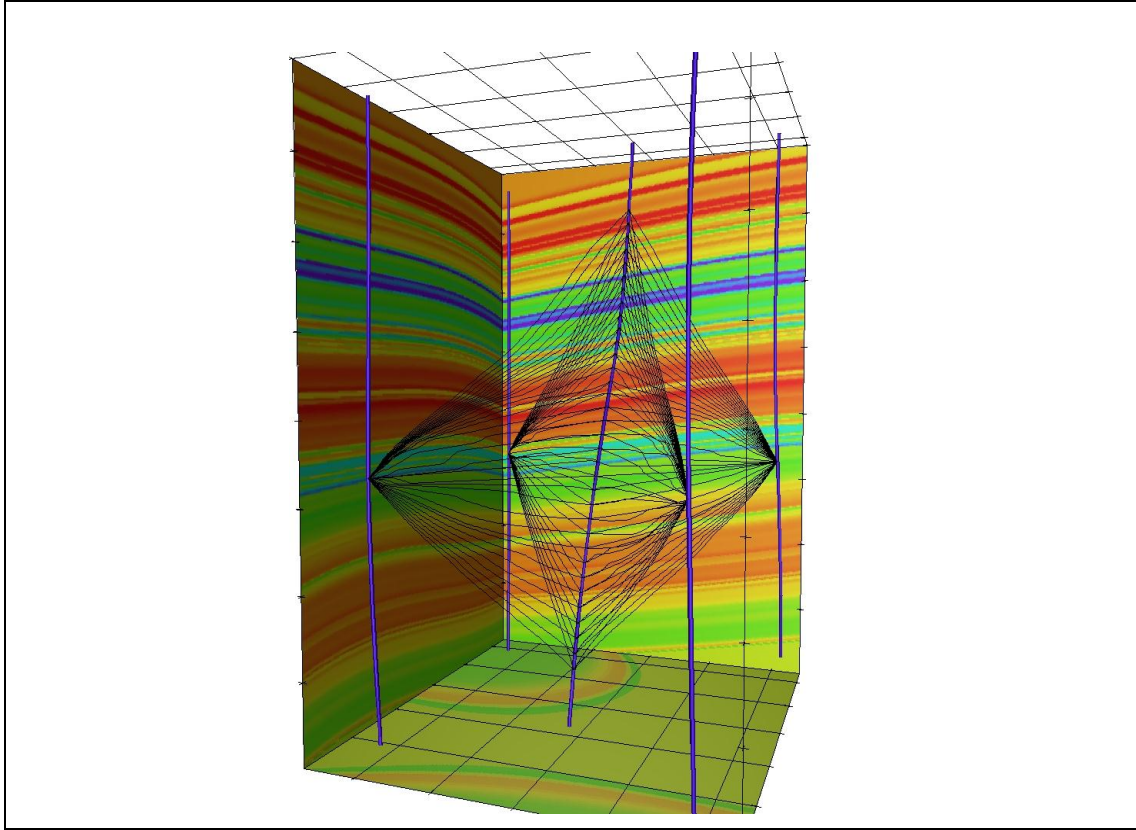


Figure III-12. A general example of a velocity model showing multiple raypaths over which the traveltimes are calculated. This example shows multiple source and receiver well pairs.

The structural model was generated by DeepLook using the horizons provided by URS/NETL for each well. Figures III-13 & III-14 show the anisotropic tomographic velocity model through each non-linear continuation step for the compressional baseline data sets. Figures III-15 & III-16 display the velocity model through each continuation step for the repeat profiles. Above each velocity model is a plot of the traveltimes residuals, which decrease with increasing iterations. As each continuation step is updated, the inversion constraints are decreased resulting in higher resolution as the iterations progress. Figures III-17 through III-20 highlight the individual time residuals for the chosen velocity models.

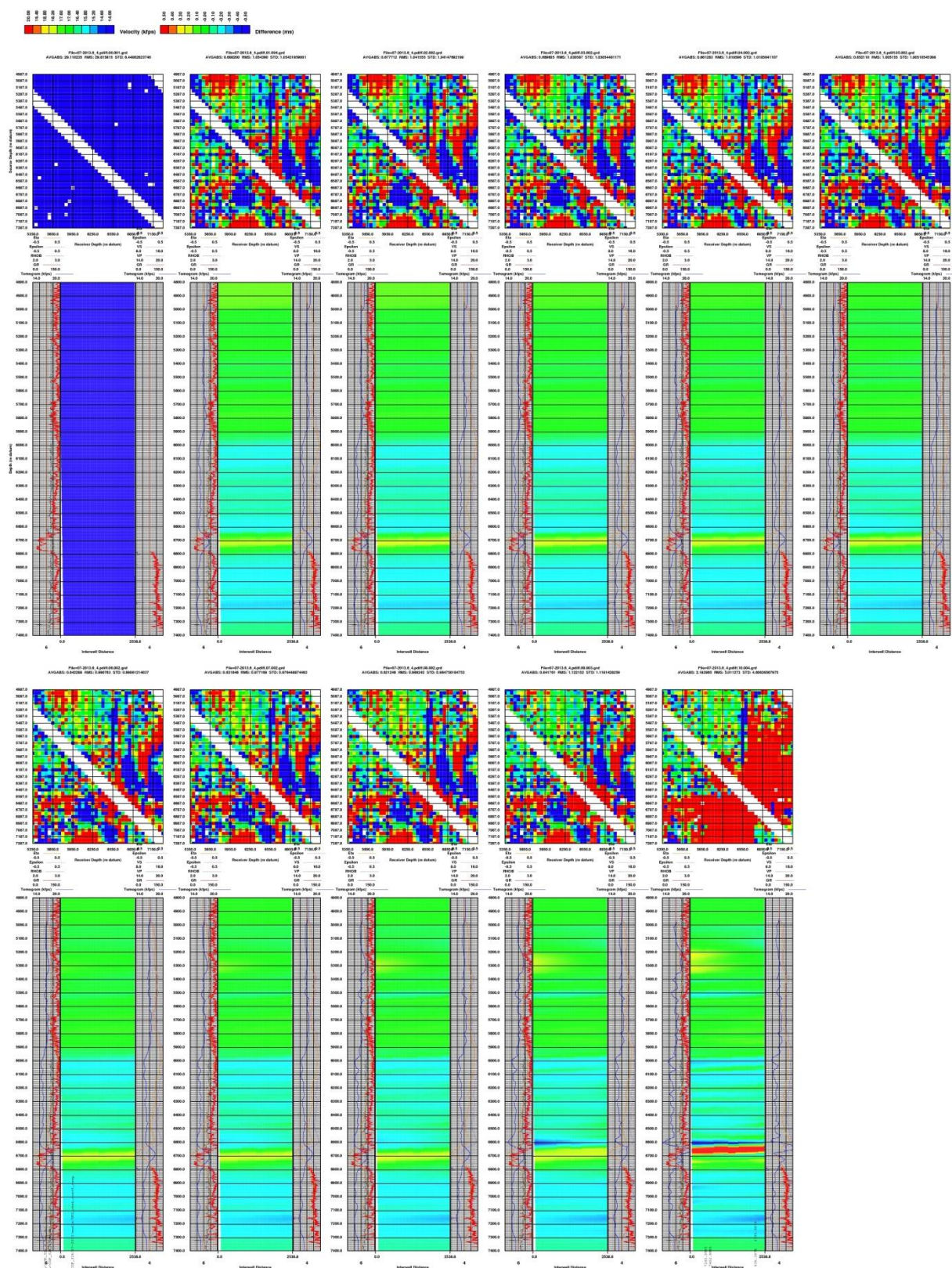


Figure III-13. Baseline Compressional Velocity Model Progression of the Traveltime Inversion.

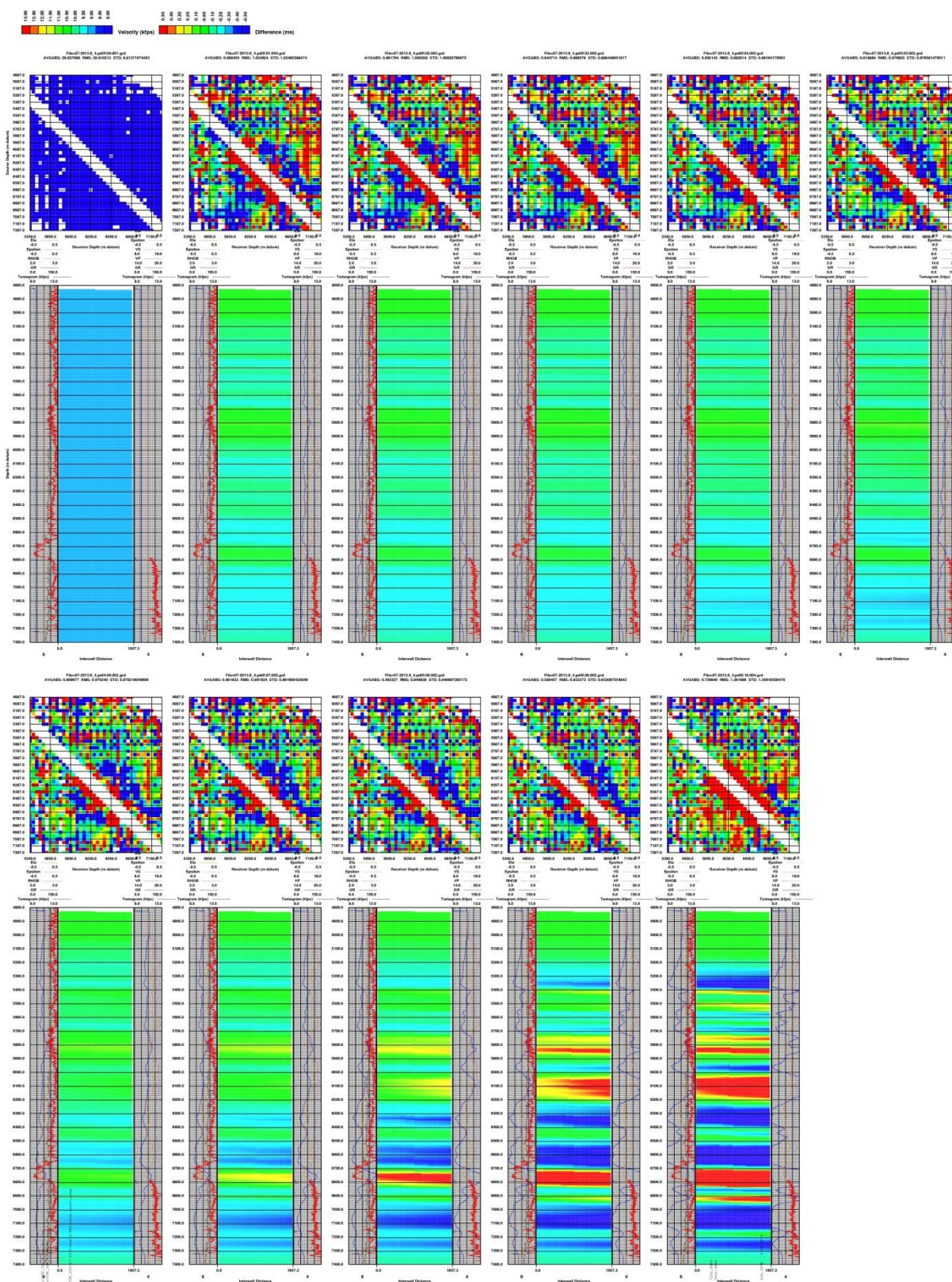


Figure III-14. Baseline Shear Velocity Model Progression of the Traveltime Inversion.

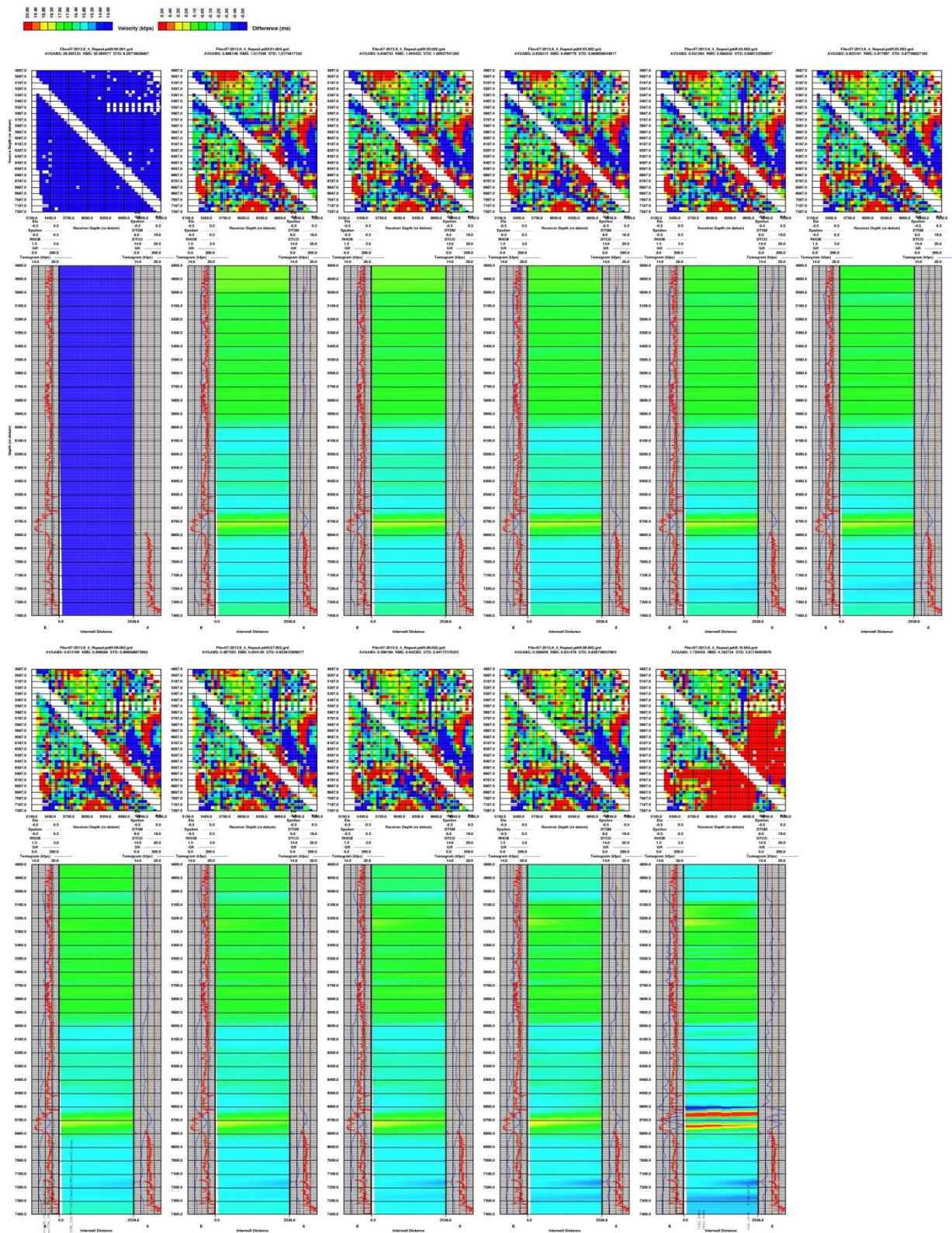


Figure III-15. Repeat Compressional Velocity Model Progression of the Traveltime Inversion.

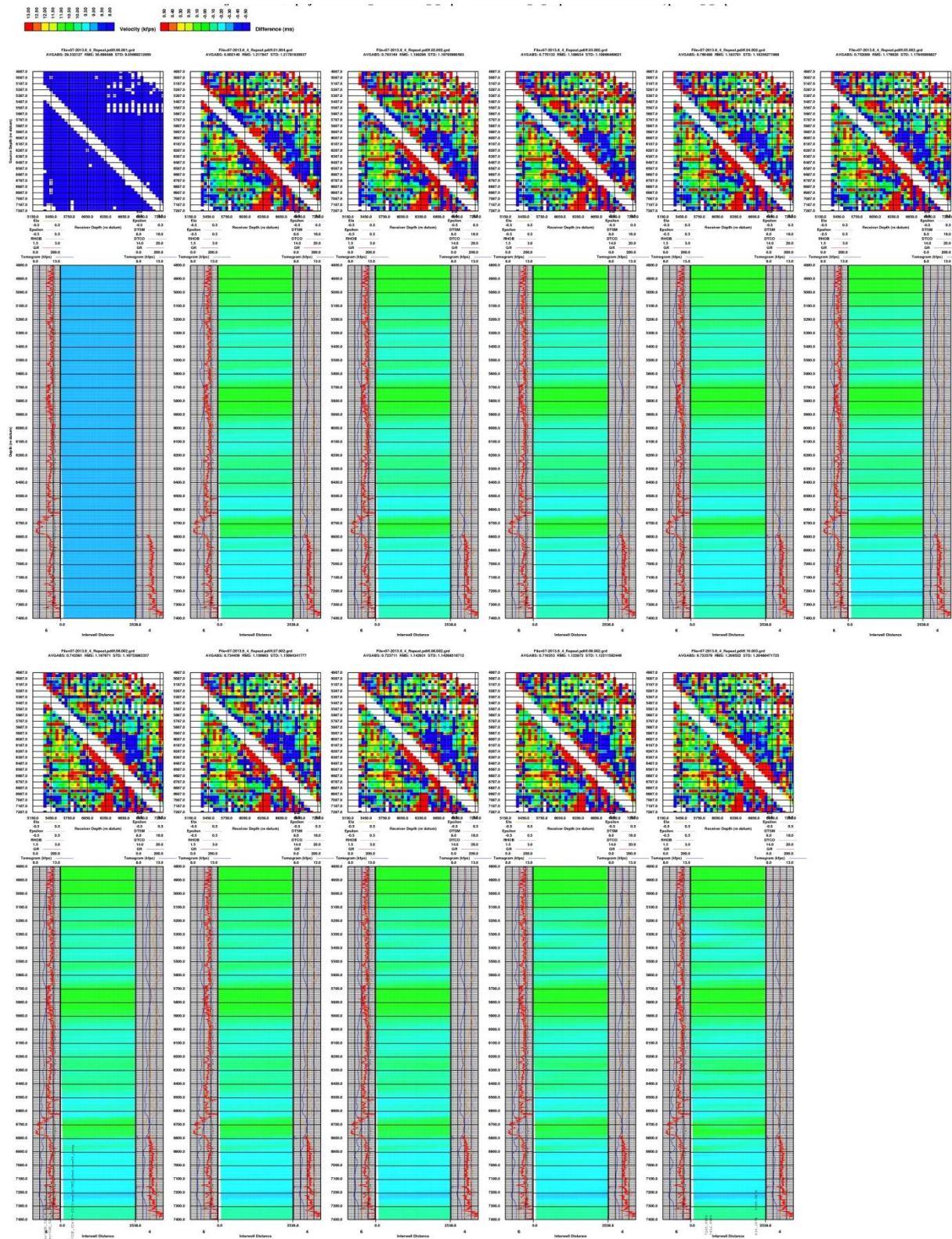


Figure III-16. Repeat Shear Velocity Model Progression of the Traveltime Inversion.

The difference between the first-arrival time picks and the ray-traced first-arrival times based on the velocity model, are displayed in Figures III-17 through III-20 for the individual anisotropic velocity results. The best tomographic inversion results show low difference values (first break – ray-traced first-arrival time), and general randomness of the difference values.

COP_324 6 - COP_324 4 Compressional Baseline Differences

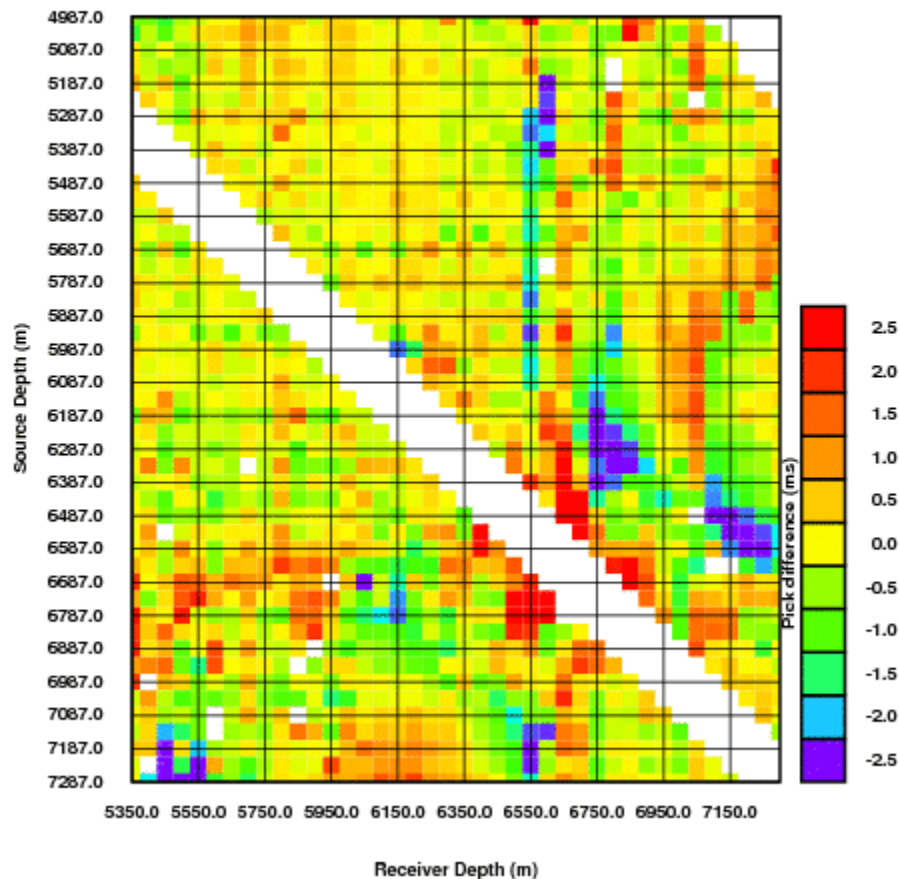


Figure III-17. Baseline Compressional Wave First-Arrival Time Residuals.

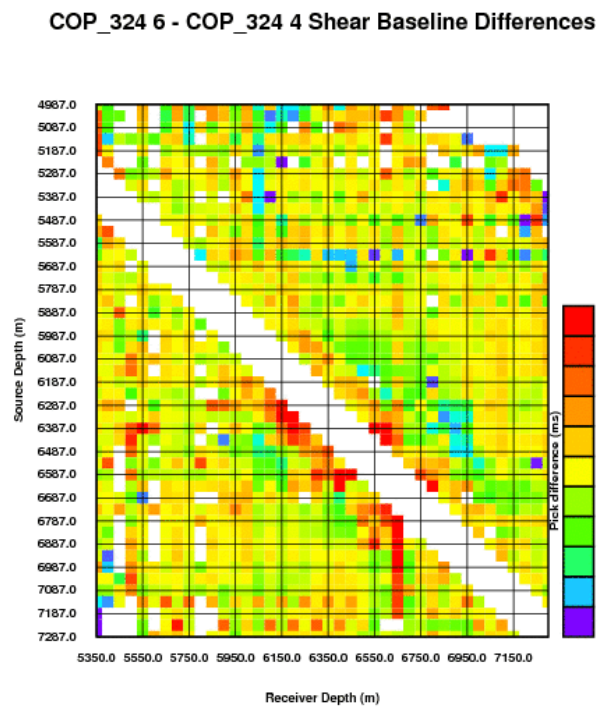


Figure III-18. Baseline Shear Wave First-Arrival Time Residuals.

COP_324 6 - COP_324 4 Compressional Repeat Differences

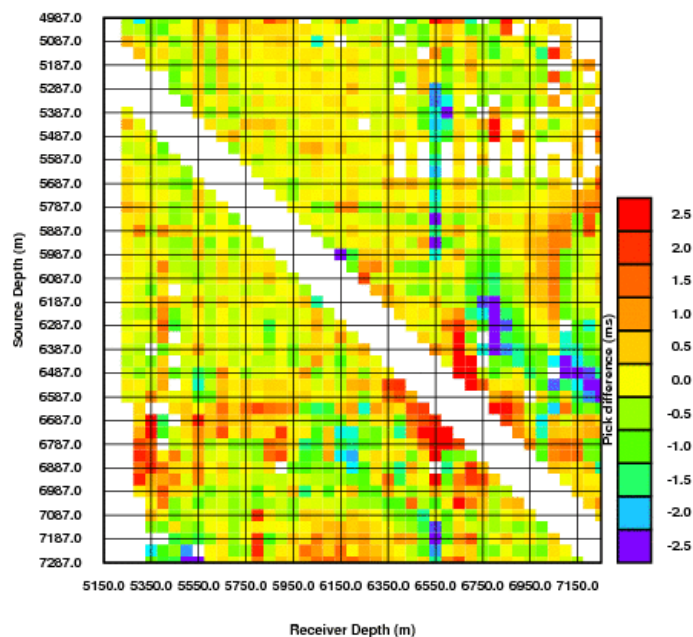


Figure III-19. Repeat Compressional Wave First-Arrival Time Residuals.

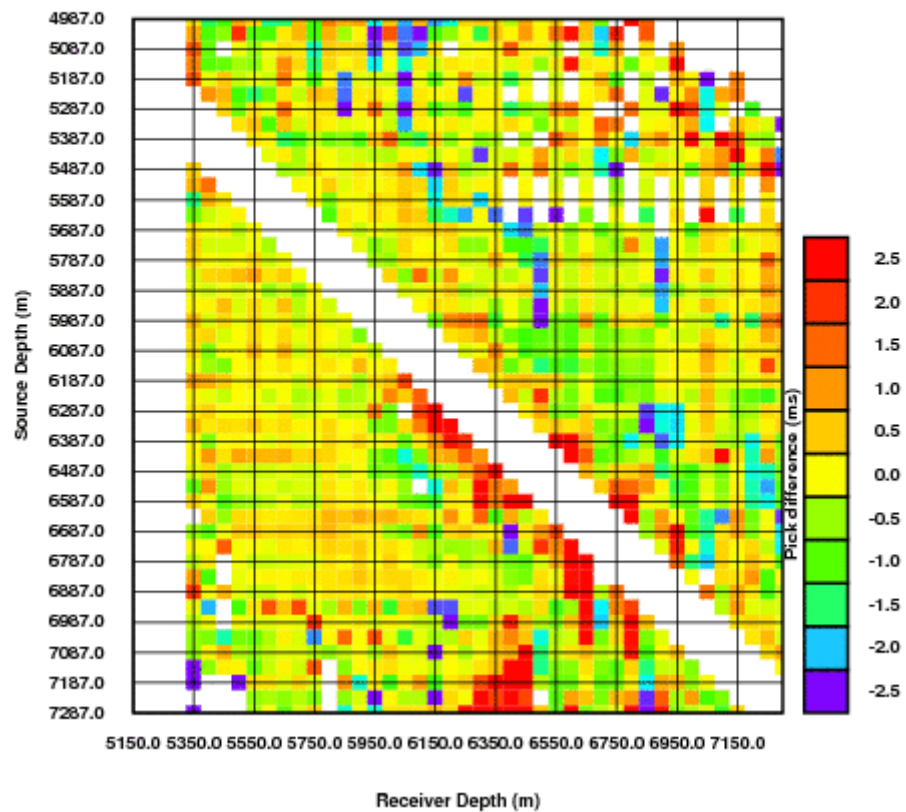
COP_324 6 - COP_324 4 Shear Repeat Differences

Figure III-20. Repeat Shear Wave First-Arrival Time Residuals.

Final Inversion

Profile COP 324#6-COP 324#4 gave good tomographic results. The final 3-D anisotropic tomograms for each of the inversion methods are displayed below in Figures III-21 through III-24.

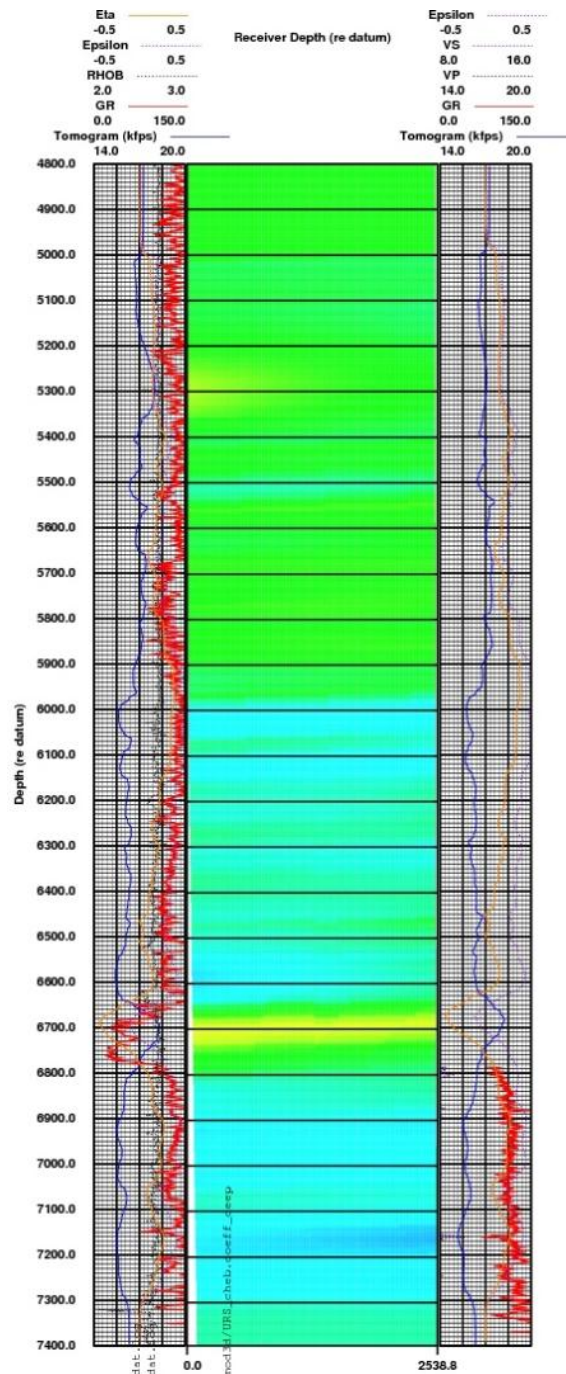


Figure III-21. Baseline Compressional Anisotropic Tomographic Velocity Model.

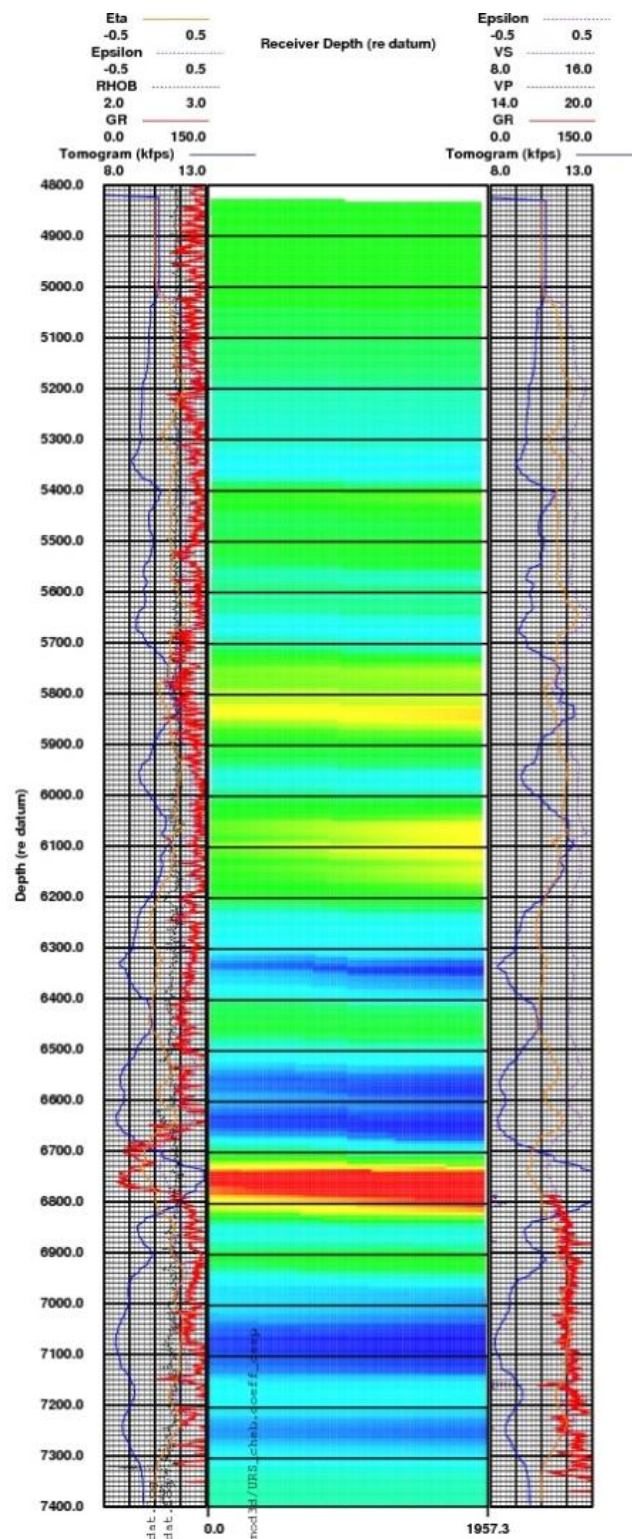


Figure III-22. Baseline Shear Anisotropic Tomographic Velocity Model.



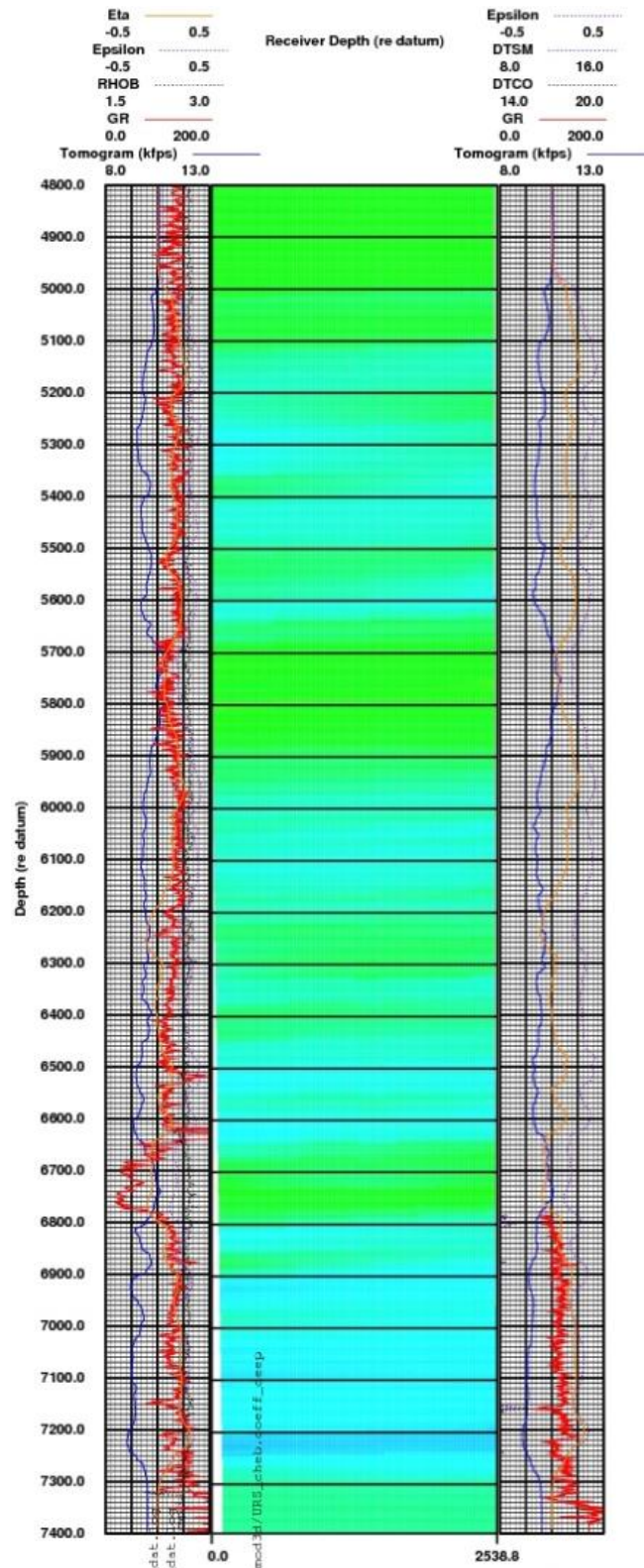


Figure III-24. Repeat Shear Anisotropic Tomographic Velocity Model.

Pixelized Difference Tomography

Pixelized difference tomography is used to image the changes in velocity during a time-lapse scenario. Figure III-25 shows the workflow for the pixelized inversion applied in COP 324. The difference tomography uses the baseline velocity tomogram and the difference between the first-arrival picks of the baseline – the repeat (Figures III-26 & III-27). The baseline tomography and the difference time picks are input to the pixelized difference tomography and an updated velocity model is generated, as well as a difference tomogram.

The pixelized inversion transforms the layering of the original structural model, defined by Chebyshev surfaces, into cells of rectangular prisms. The cells have regular horizontal boundaries and potentially curved surfaces for vertical boundaries. Generally, the direct-arrival and reflection tomography inversions provide excellent vertical resolution, however the lateral resolution of the tomograms are very limited. An inversion based on a pixelized format allows for an increase in the lateral resolution of the tomograms, resulting in better identification of velocity changes within the source and receiver wells.

Pixelized tomography uses the raypaths already described by the previous inversion through the Chebyshev model. This advantage allows perform multiple inversions with different parameters. The correct definition of pair of vertical and horizontal constraints is fundamental during the execution of this type of inversion.

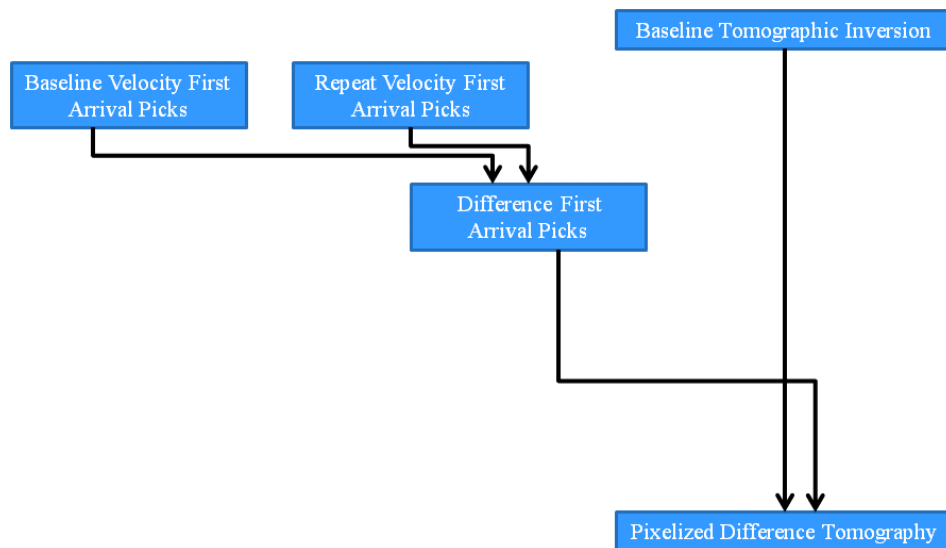


Figure III-25. Pixelized Inversion Flow.

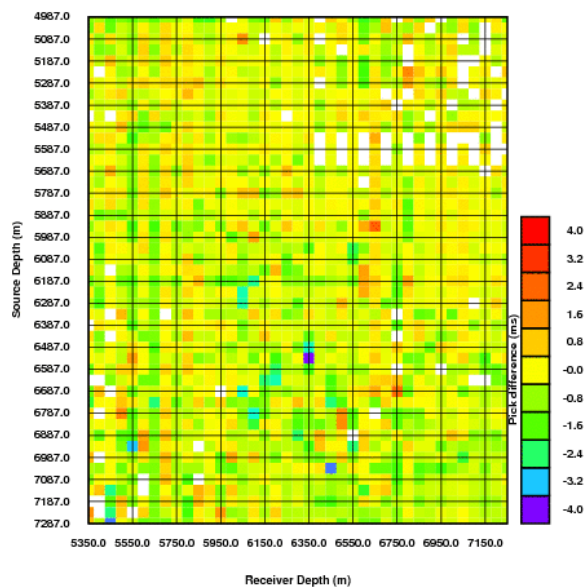
COP_324 6 - COP_324 4 Compressional Time Differences

Figure III-26. Compressional First-Arrival Traveltime Pick Difference

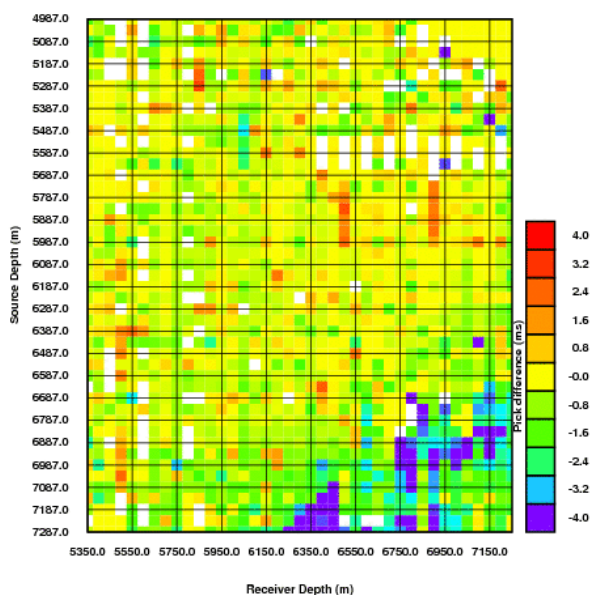
COP_324 6 - COP_324 4 Shear Time Differences

Figure III-27. Shear First-Arrival Traveltime Pick Difference

The results of the pixelized tomography are presented in Figure III-28 & III-29. The upper left panel in the image represents the baseline velocities. Moving clockwise, the upper right panel corresponds to the updated velocities, while the lower panels show the percent velocity change on the right and the velocity change on the left.

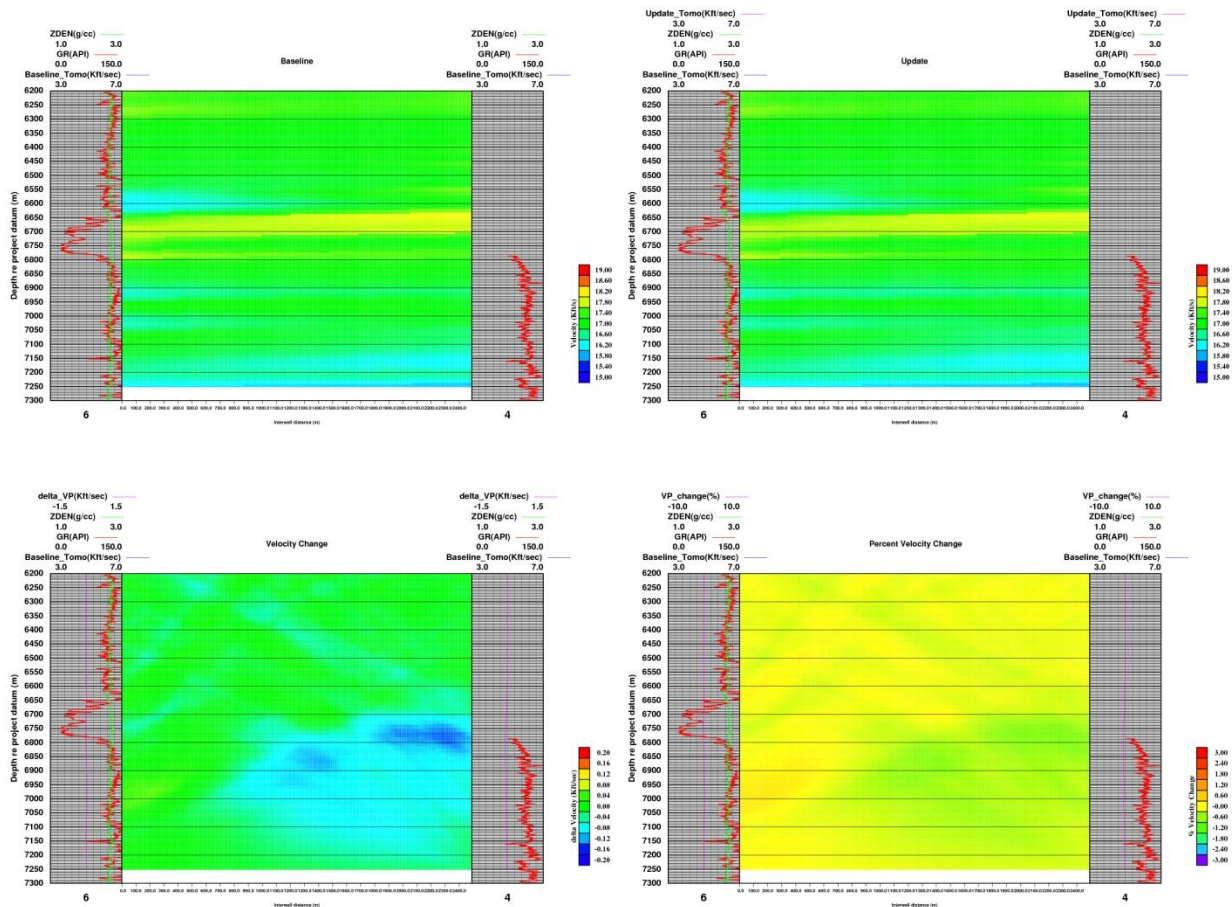


Figure III-28. Compressional Difference Tomography Results

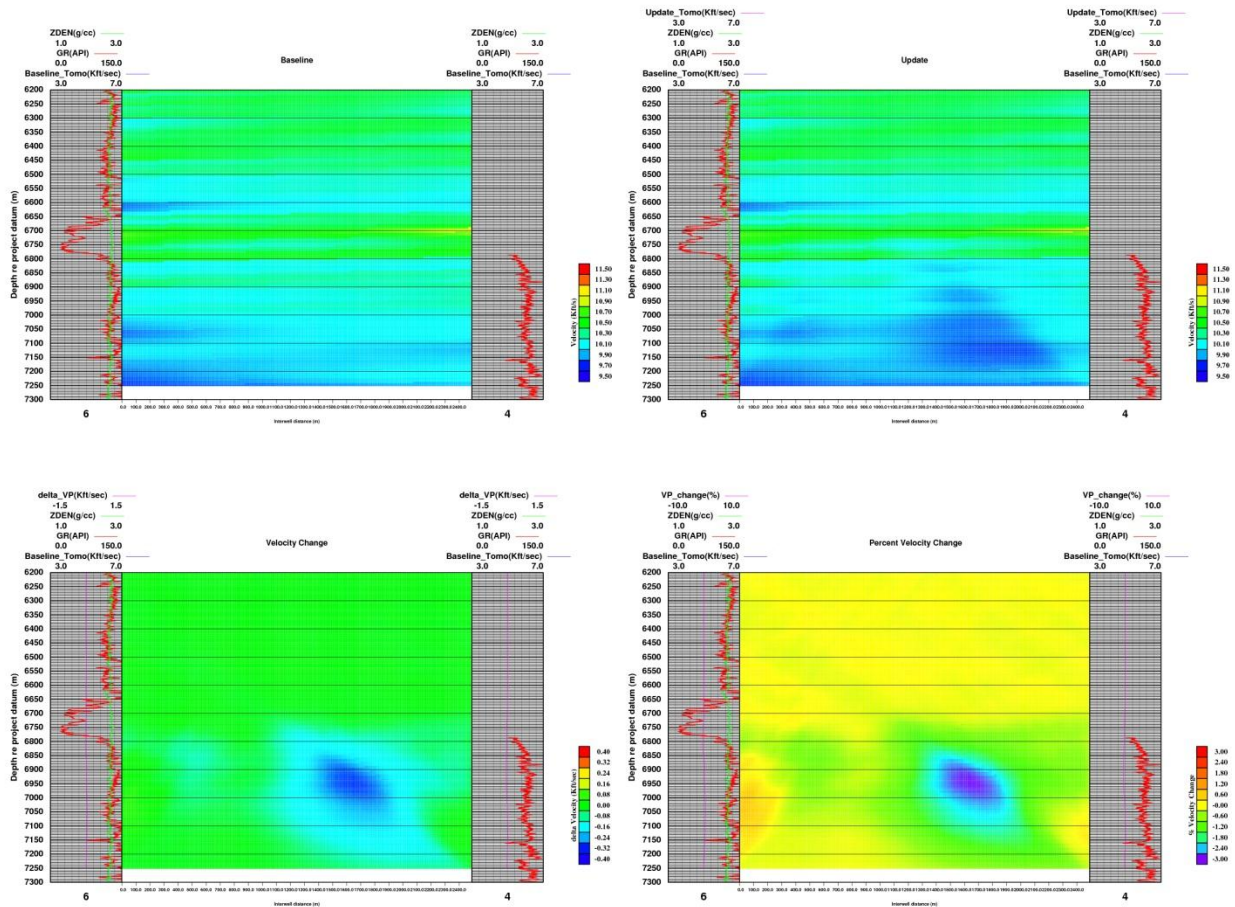


Figure III-29. Shear Difference Tomography Results

Reflection Imaging

For a detailed description of reflection imaging processes, please see Appendix B. Figure III-30 is a flow chart of the steps involved in crosswell seismic data processing for reflection imaging.

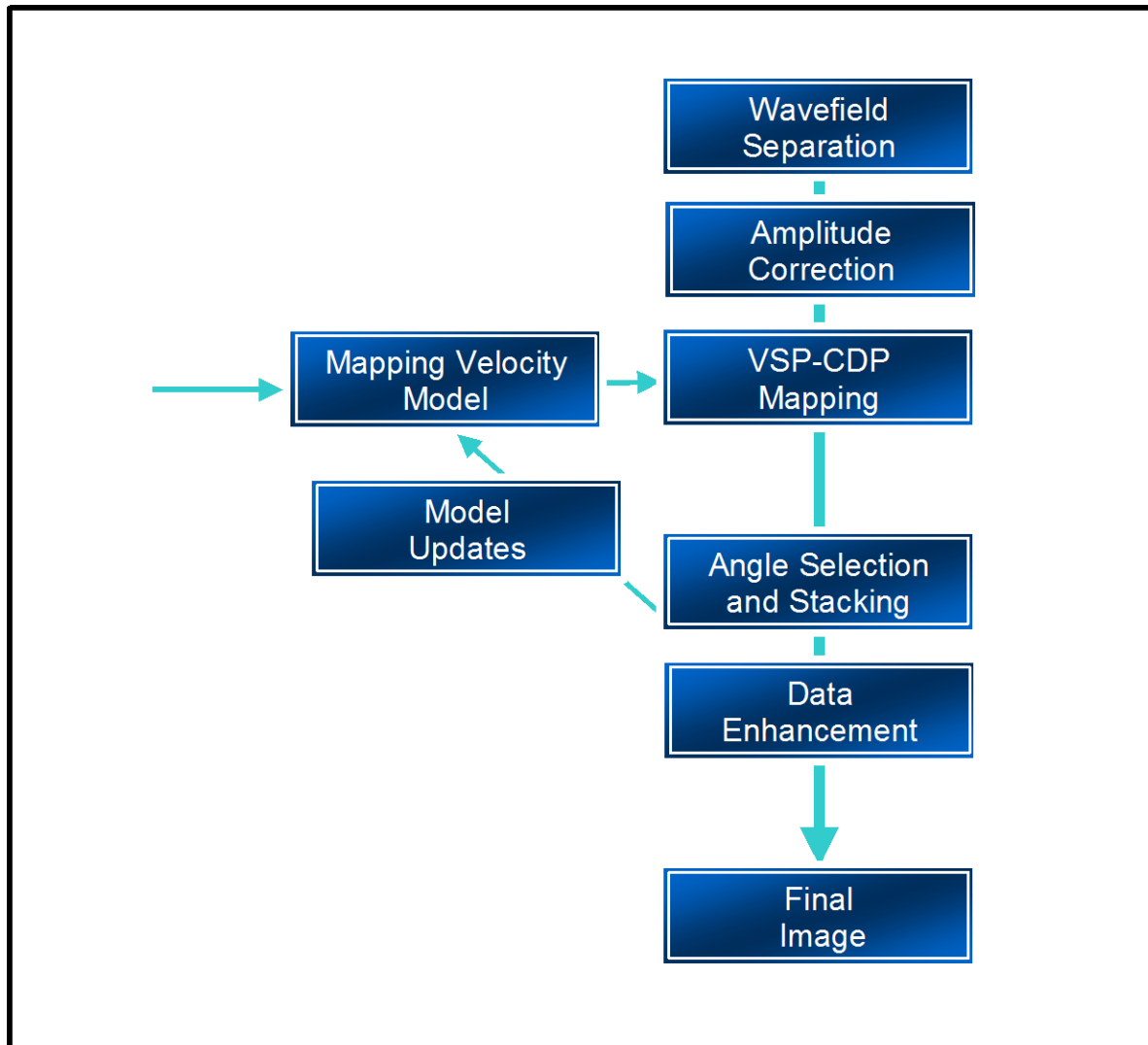


Figure III-30. Reflection Imaging Workflow.

In crosswell data, there are many arrivals present in the wavefield: direct arrivals, P and S reflections from below (up-going) and above (down-going) the source and receiver, as well as various converted modes and tubewaves. For reflection imaging of the reservoir interval, the objective was to use the up-going P-wave reflections. All arrivals in the wavefield that contribute coherent noise to the final stacked image are removed through spatial filtering.

Wavefield Separation

Prior to transforming the time-domain data into a data volume in depth, the data are filtered to remove coherent modes that do not stack out of the final image. The resulting filtering leaves up-coming reflection energy only. The unwanted modes are attenuated using spatial filters, usually f - k fan filters or variations of median filters, applied in common-receiver gather (CRG), common-source gather (CSG), and common-offset gathers (COG).



The usual approach is to filter the largest noise mode in the data first. This result is evaluated by mapping and stacking, and the next largest noise mode is then removed. This procedure is repeated until all separable noise modes have been attenuated. The final step is to remove the unwanted reflection energy. In the case of up-going reflection imaging, this is the down-going reflection energy. This is typically the final time-domain filter before mapping. The filter used to remove down-going reflections was a half-space f - k fan filter applied in CRG followed by CSG. These filtered data are then deconvolved, amplitude corrected, and mapped to depth using a VSP-CDP transform.

The direct-arrival was aligned to the zero moveout in COGs using the first-arrival traveltimes picks. Each trace was scaled by the RMS amplitude on a window centered on the direct-arrival prior to applying an f - k fan reject filter. After filtering, the gain and time delay of the trace was restored.

Next, all down-going energy was removed using an f - k fan filter to remove the down-going half-space first in the CRGs, then the CSGs. The same common-source and receiver gathers following direct-arrival and down-going removal are shown in Figures III-31 through III-38.

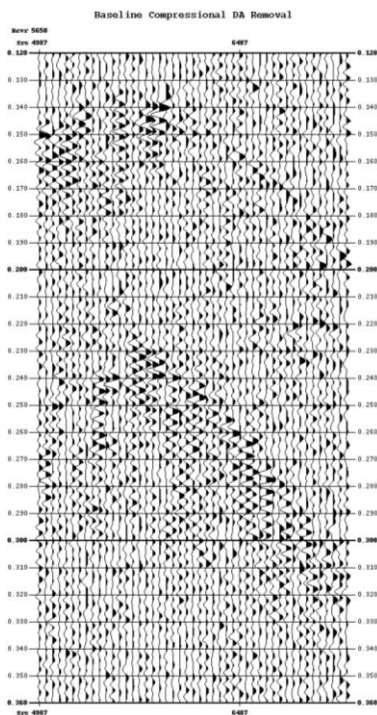


Figure III-31. Baseline Compressional Common-Receiver Gather after Direct Arrival Removal.

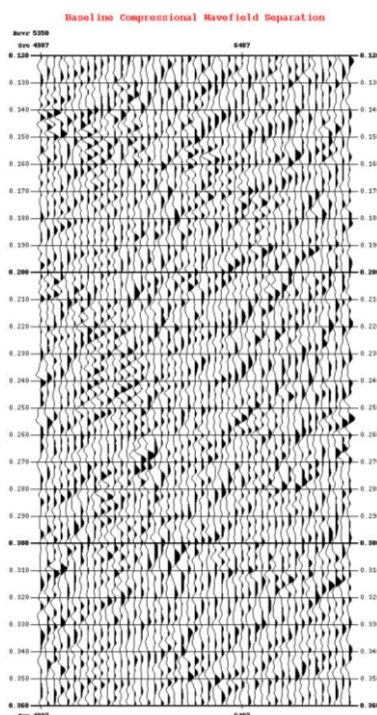


Figure III-32. Baseline Compressional Common-Receiver Gather after Wavefield Separation.

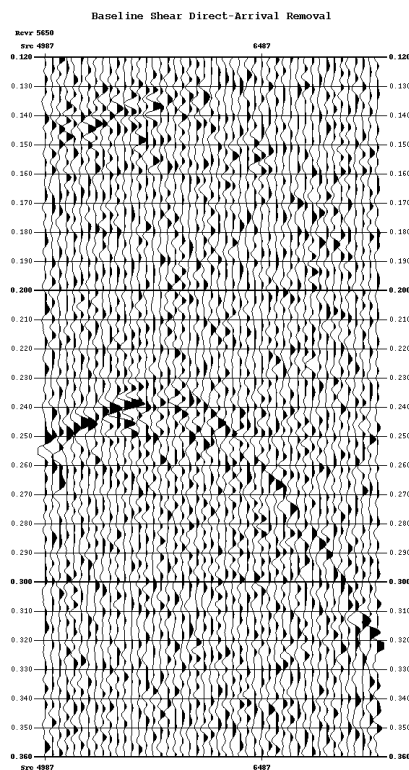


Figure III-33. Baseline Shear Common-Receiver Gather after Direct Arrival Removal.

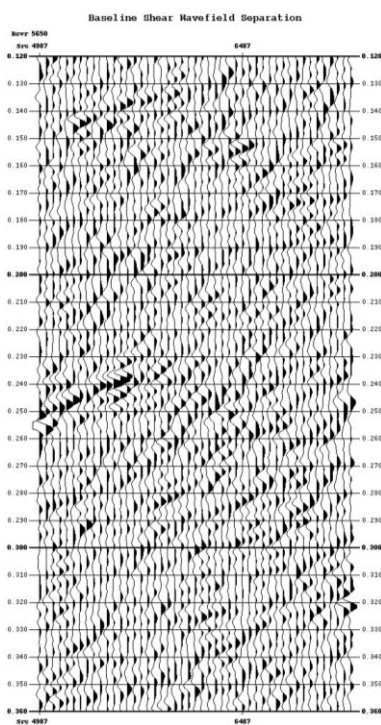


Figure III-34. Baseline Shear Common-Receiver Gather after Wavefield Separation.

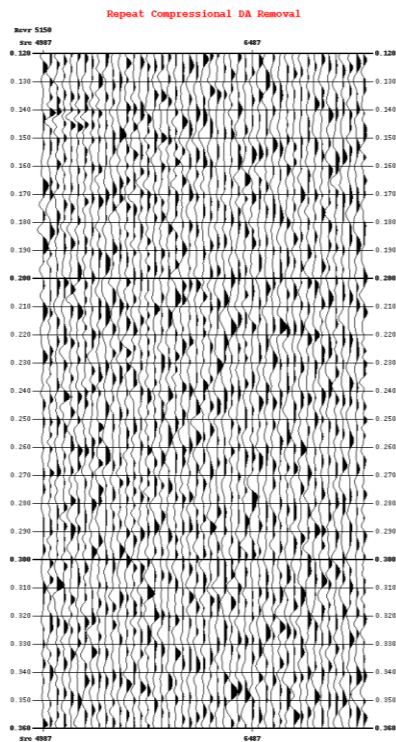


Figure III-35. Repeat Compressional Common-Receiver Gather after Direct Arrival Removal.

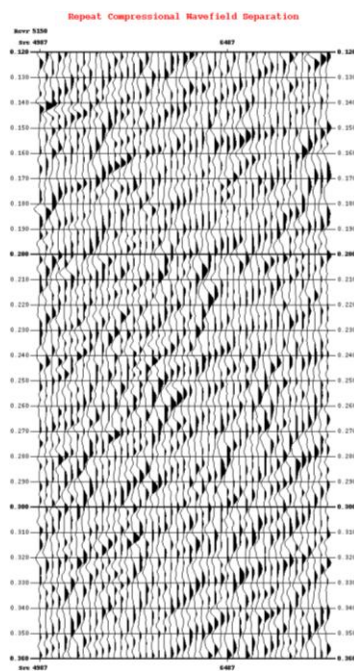


Figure III-36. Repeat Compressional Common-Receiver Gather after Wavefield Separation.

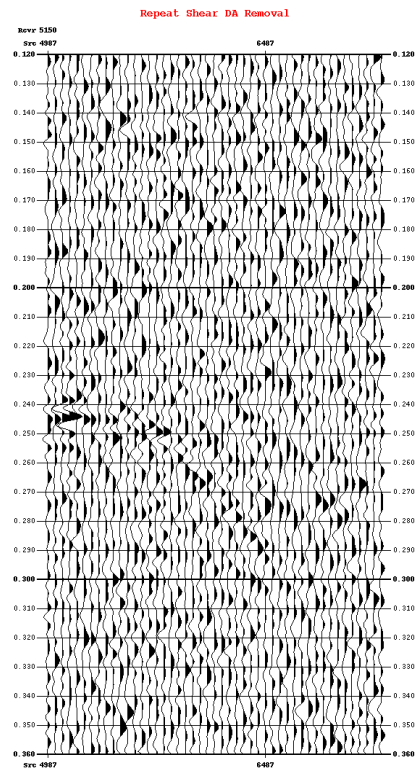


Figure III-37. Repeat Shear Common-Receiver Gather after Direct Arrival Removal.

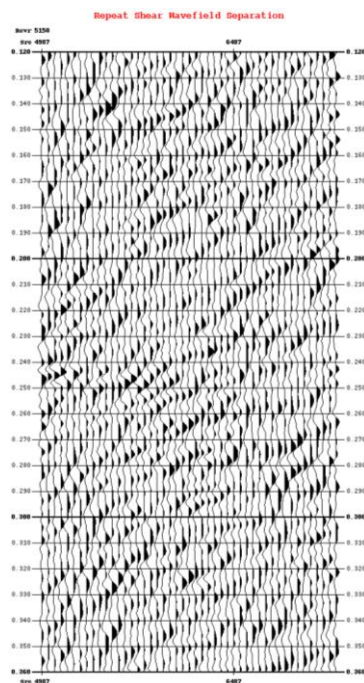


Figure III-38. Repeat Shear Common-Receiver Gather after Wavefield Separation.

Deconvolution and Amplitude Normalization

The wavefield-separated data were deconvolved with a zero-phase spiking filter. The deconvolution operator was calculated for a window from 10ms before and 100ms after the direct-arrival time with 10% white light using a filter length of 150ms. The data were then gained.

The reflection amplitudes recorded in crosswell data are affected by several factors that are not related to the reflection coefficient of a reflecting horizon. The goal of amplitude normalization is to correct the amplitudes of the time-domain data before mapping so the resulting reflection images have reflection events of the correct amplitude. Coupling, radiation pattern, and wellbore impedance are several factors affecting the amplitude of the recorded seismic data.

The amplitude normalization used was a trace balance computed trace-by-trace over the time window 10ms before the first-arrival time to 100ms after the first-arrival time.

Figures III-39 through III-42 show a receiver gather, for both the compressional and shear arrivals for the baseline and repeat profiles, with deconvolution and gain applied.

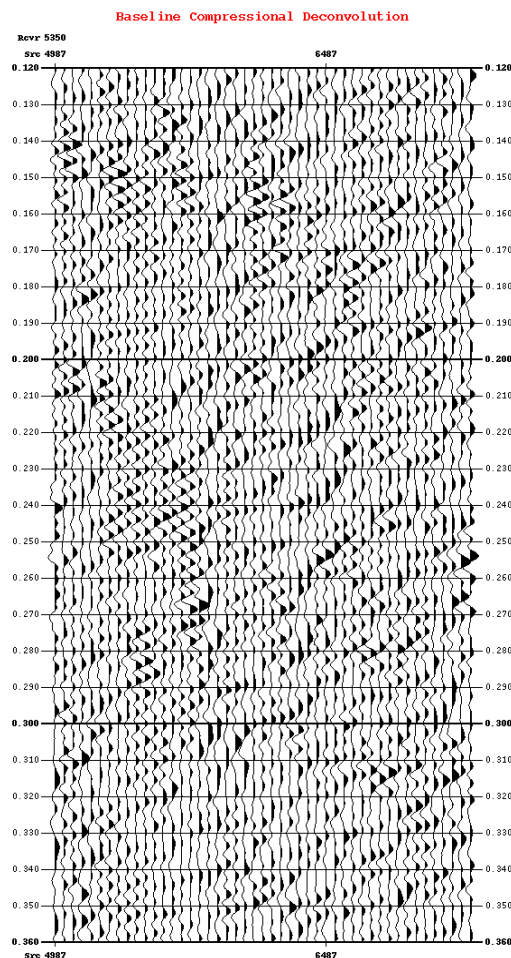


Figure III-39. Baseline Compressional Common-Receiver Gather with Gain, Normalization, and Deconvolution Applied.

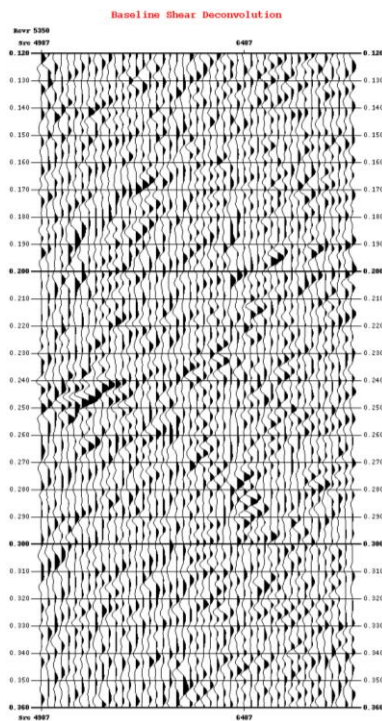


Figure III-40. Baseline Shear Common-Receiver Gather with Gain, Normalization, and Deconvolution Applied.

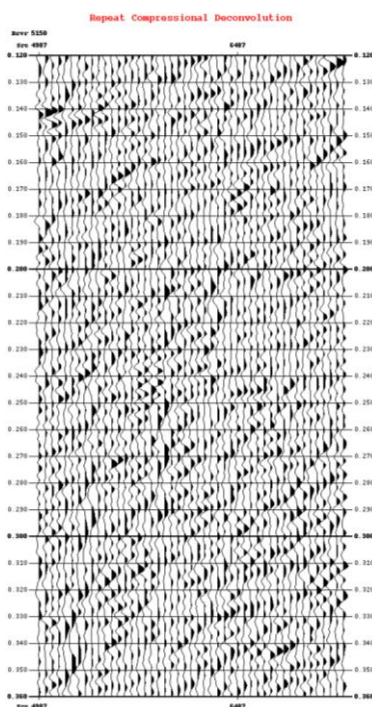


Figure III-41. Repeat Compressional Common-Receiver Gather with Gain, Normalization, and Deconvolution Applied.

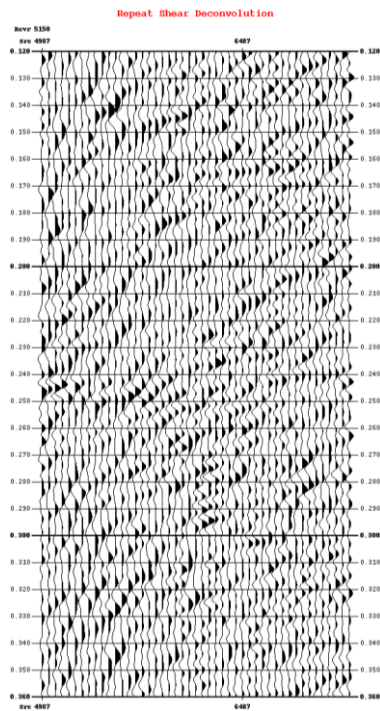


Figure III-42. Repeat Shear Common-Receiver Gather with Gain, Normalization, and Deconvolution Applied.

VSP-CDP Mapping/Time-Depth Conversion

The wavefield-separated data were then VSP-CDP depth mapped, as in Offset-VSP data processing. The velocity model from the traveltime inversion was used in tracing reflection raypaths. The VSP-CDP mapped data set is a 3-D data cube with mid-depth and offset (distance between the wells) as the two axes. Individual depth-mapped mid-depth gathers were reviewed and compared to the time-domain data to ensure that the stacked image contained only events with reflection moveouts.

Post-Map Migration

The mapped data were then post-map migrated. Each VSP-CDP transformed mid-depth gather is migrated. This yields a set of migrated mid-depth gathers, which are stacked in order to provide a final migrated reflection image. The migration was aperture limited by angles of -10 degrees to +10 degrees.

Angle Selection and Stacking

Since there are a wide range of incidence angles present on a crosswell data set and the wavelet and reflection character change with incidence angle, another natural domain for data analysis is the angle-transformed Amplitude Versus Angle (AVA) data cube shown in Figure III-43.

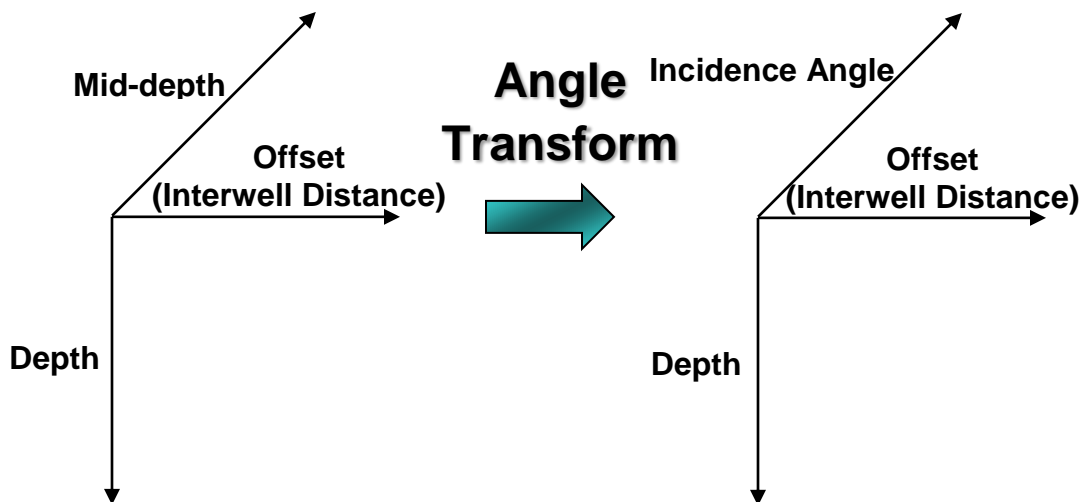


Figure III-43. Schematic of the Angle Transform.

Angle selection was used to select angles that maintain adequate SNR, while best approximating the vertical incidence (0°) response. Reflection events should be flat in AVA gathers. Small velocity errors may result in dips for events in AVA gathers. Figure III-44 displays example angle gather from the compressional up-coming wavefield data with deconvolution, using the anisotropic velocity model.

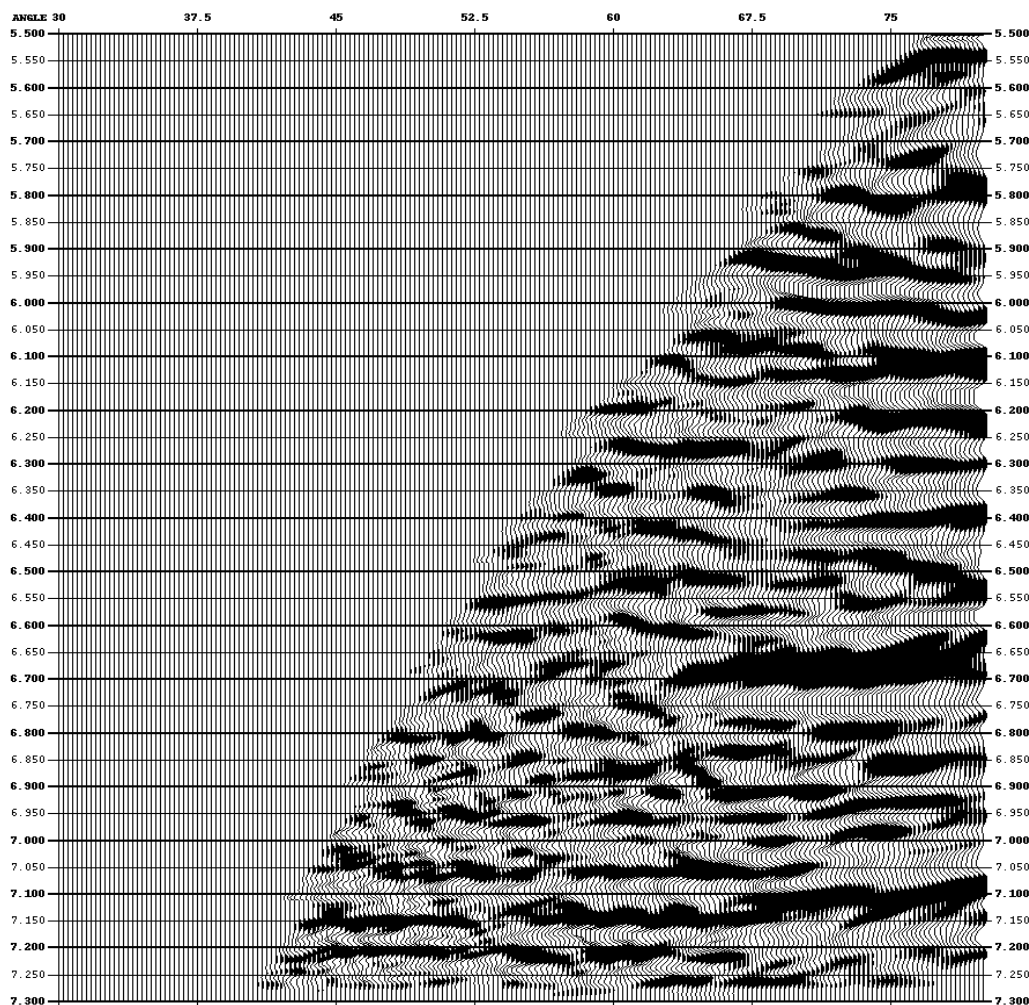


Figure III-44. Baseline Compressional AVA Gather.

Because crosswell reflection data has incidence angles approaching 90 degrees, care was taken to not include post-critical angles in the final reflection stack. The final stacking angle range was 55 to 70 degrees. Angle limited reflection stacks were also created for URS/NETL and displayed.

Data Enhancement

A depth-domain Ormsby bandpass filter of 0-1-60-65 cycles/Kft was applied to enhance the reflection events. In addition, a final trace balance over the entire trace length was applied to the data to gain up the edges of the image, which have low amplitude due to the limited migration aperture at the edges. Table III-I summarizes the post processing parameters used to enhance the final images. Figures III-45 through III-52 summarize the final results for the URS/NETLCOP 324 project.

URS/NETL COP 324 Post-Processing Parameters COP 324#6-COP 324#4	
Angle Range for Stack (degrees from vertical)	55-70
Depth Domain Bandpass Filter (cycles/km)	0-1-60-65
Trace Mix	9
Normalization	Trace by Trace
Plotting Trace increment	2

Table III-1: Post-Processing Parameters.

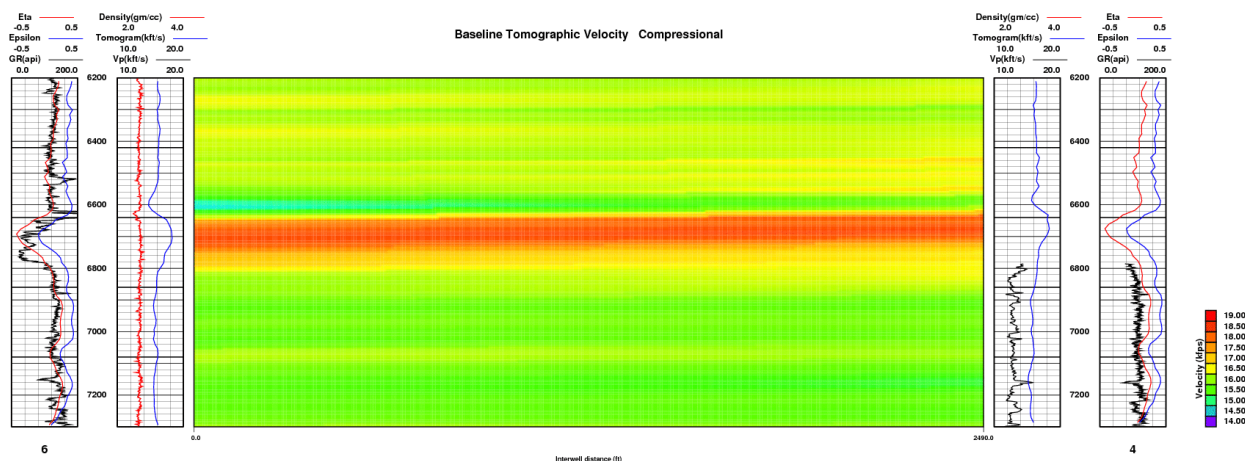


Figure III-45. Baselines Compressional Tomographic Results.

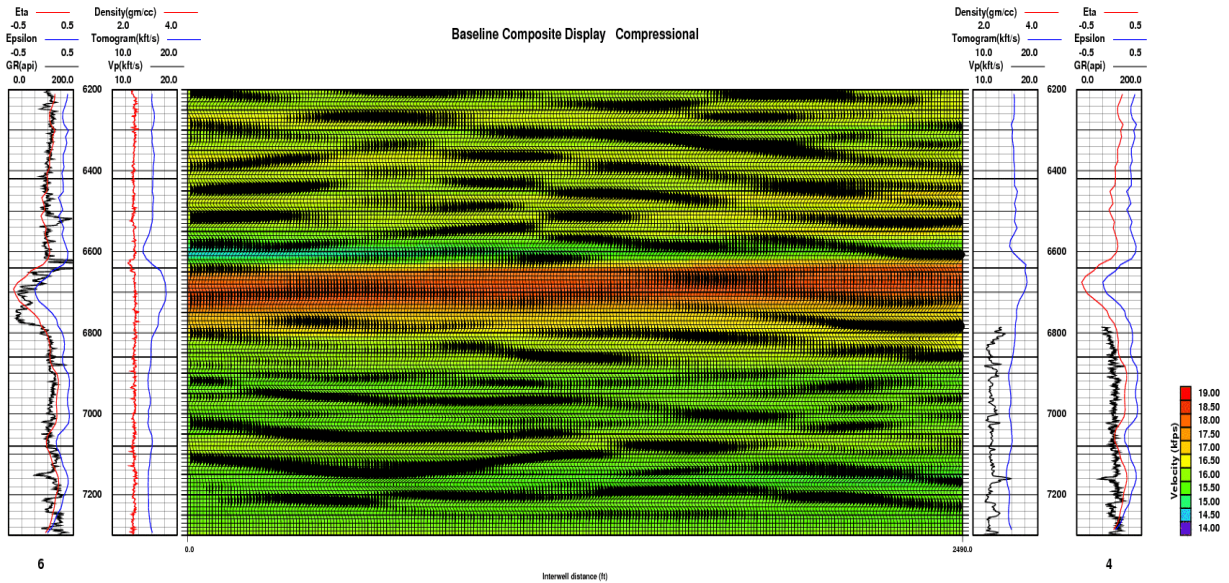


Figure III-46. Baselines Compressional Composite Results.

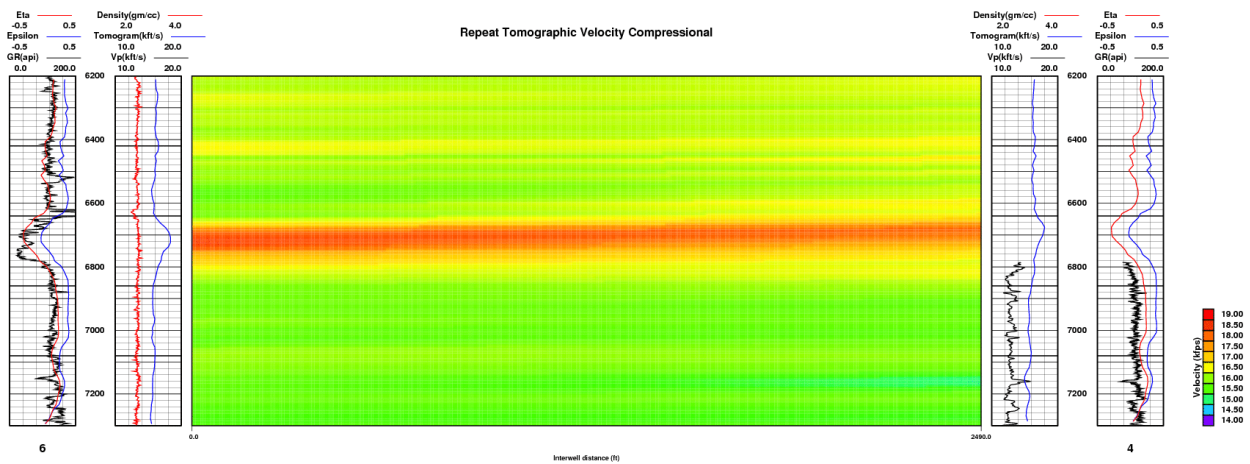


Figure III-47. Repeat Compressional Tomographic Results.

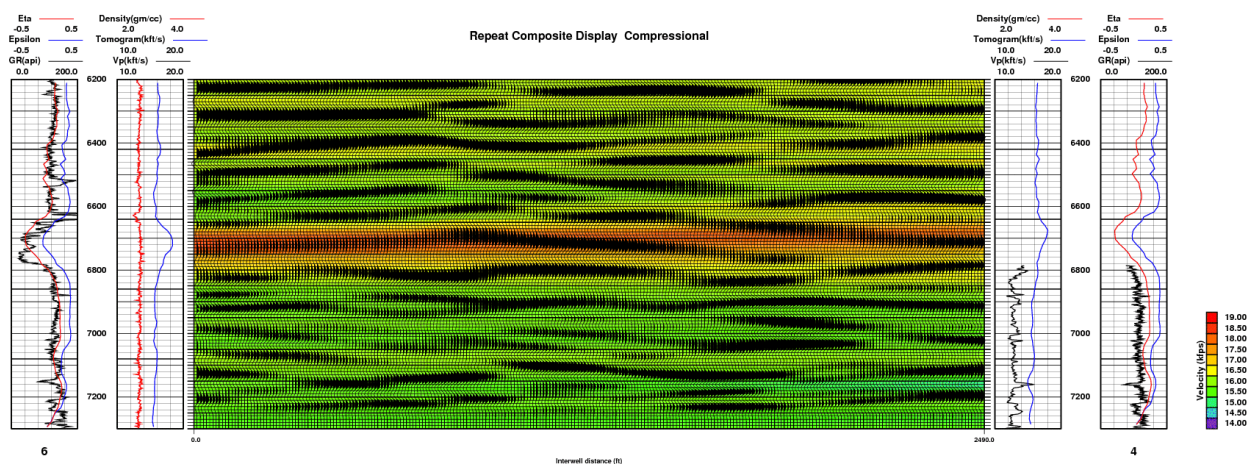


Figure III-48. Repeat Compressional Composite Results.

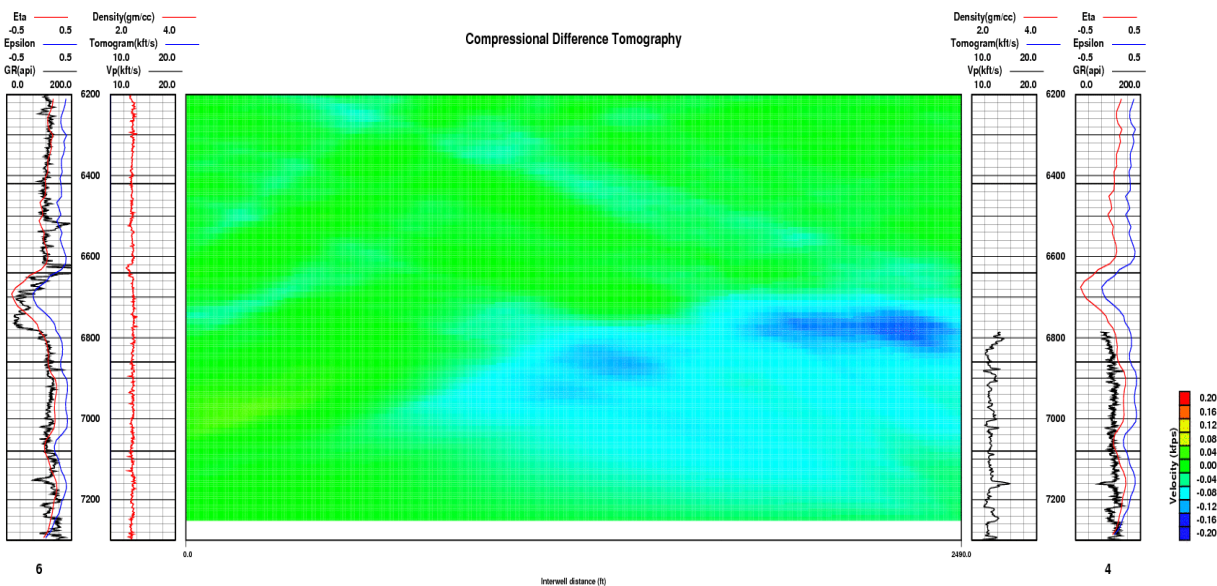


Figure III-49. COP 324#6-COP 324#4 Compressional Pixelized Difference Tomography Results.

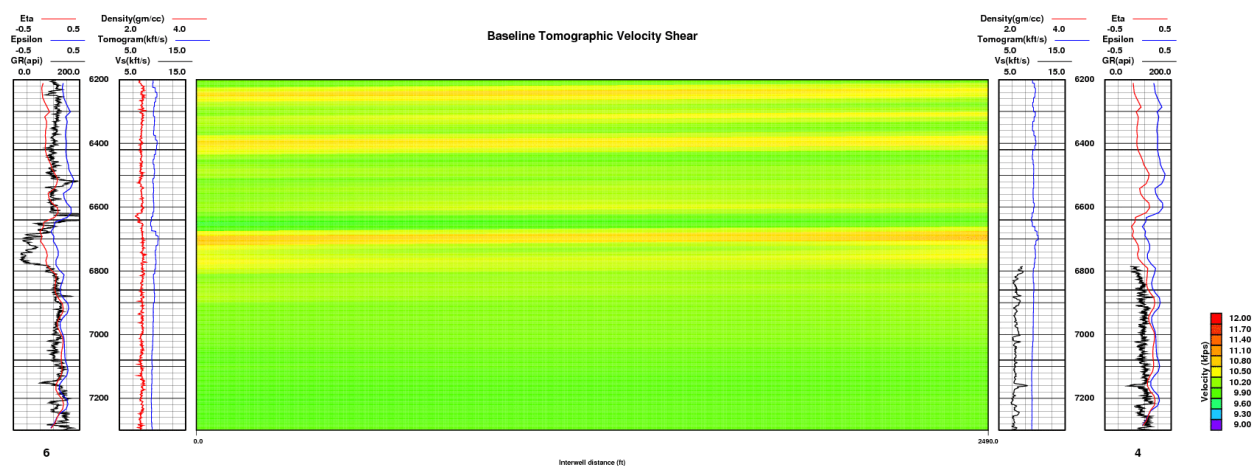


Figure I-50. Baseline Shear Tomographic Results.

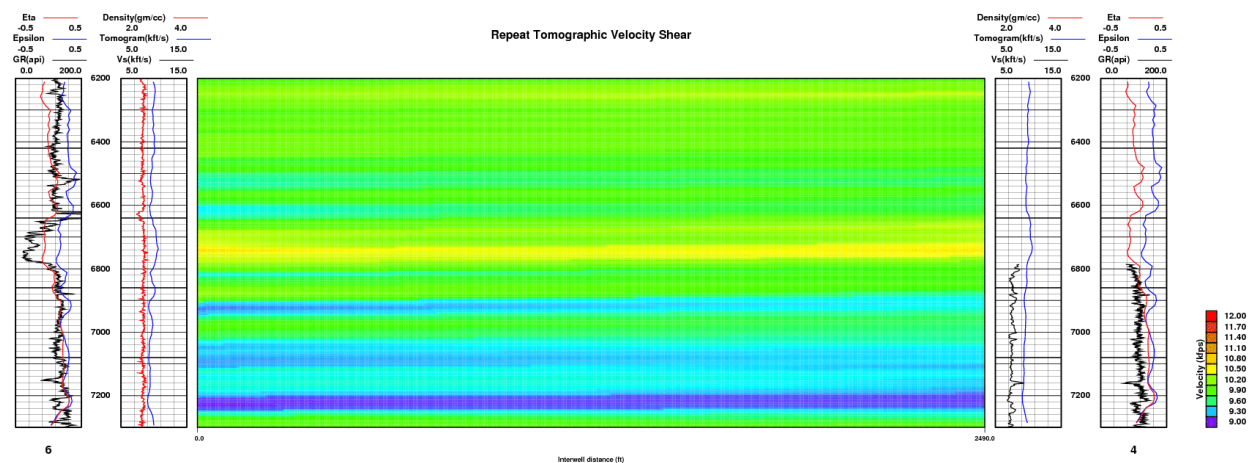


Figure I-51. Repeat Shear Tomographic Results.

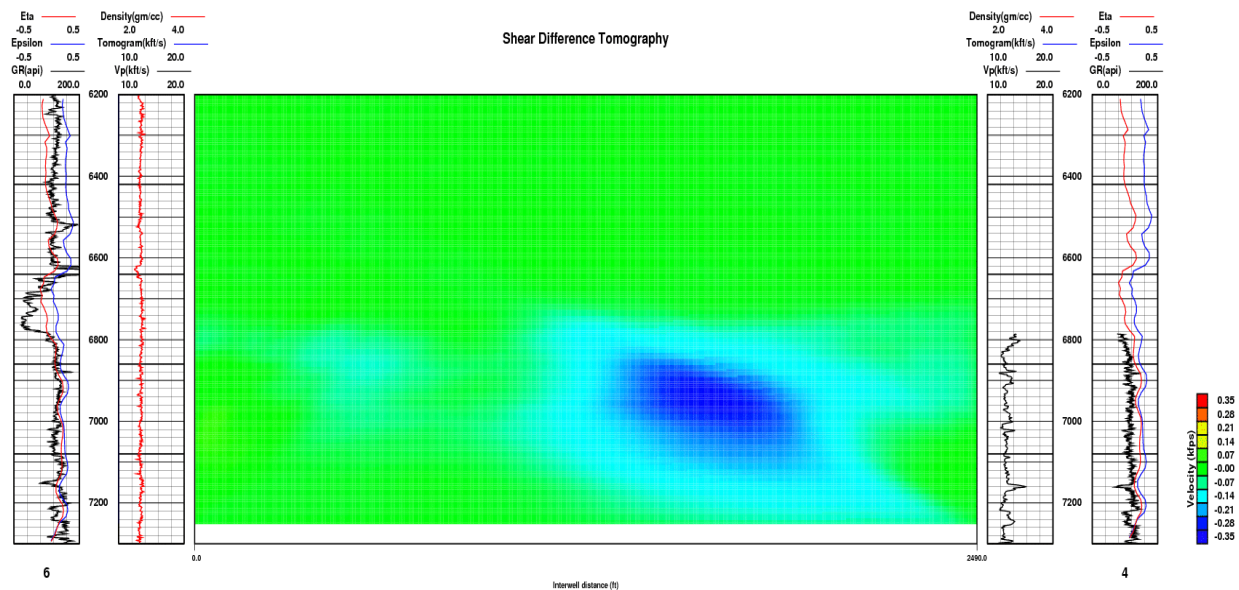


Figure III-52. COP 324#6-COP 324#4 Shear Pixelized Difference Tomography Results.

APPENDIX A – TOMOGRAPHIC INVERSION

APPENDIX B – REFLECTION IMAGING

APPENDIX C – ANISOTROPY PROCESSING

APPENDIX D – SURVEY LOGS

CROSSWELL METHODS AND GLOSSARY